J. Fluid Mech. (1991), *vol.* 226, *pp.* 511–547
Printed in Great Britain

Chaos in a model of forced quasi-geostrophic flow over topography: an application of Melnikov's method

By J. S. ALLEN[1], R. M. SAMELSON[2] AND P. A. NEWBERGER[1]

[1] College of Oceanography, Oregon State University, Oceanography Admin. Bldg 104, Corvallis, OR 97331-5503, USA

[2] Woods Hole Oceanographic Institution, Woods Hole, MA 02543, USA

(Received 20 February 1990 and in revised form 15 November 1990)

We demonstrate the existence of a chaotic invariant set of solutions of an idealized model for wind-forced quasi-geostrophic flow over a continental margin with variable topography. The model (originally formulated to investigate mean flow generation by topographic wave drag) has bottom topography that slopes linearly offshore and varies sinusoidally alongshore. The alongshore topographic scales are taken to be short compared to the cross-shelf scale, allowing Hart's (1979) quasi-two-dimensional approximation, and the governing equations reduce to a non-autonomous system of three coupled nonlinear ordinary differential equations. For weak (constant plus time-periodic) forcing and weak friction, we apply a recent extension (Wiggins & Holmes 1987) of the method of Melnikov (1963) to test for the existence of transverse homoclinic orbits in the model. The inviscid unforced equations have two constants of motion, corresponding to energy E and enstrophy M, and reduce to a one-degree-of-freedom Hamiltonian system which, for a range of values of the constant $G = E - M$, has a pair of homoclinic orbits to a hyperbolic saddle point. Weak forcing and friction cause slow variations in G, but for a range of parameter values one saddle point is shown to persist as a hyperbolic periodic orbit and Melnikov's method may be applied to study the perturbations of the associated homoclinic orbits. In the absence of time-periodic forcing, the hyperbolic periodic orbit reduces to the unstable fixed point that occurs with steady forcing and friction. The method yields analytical expressions for the parameter values for which sets of chaotic solutions exist for sufficiently weak time-dependent forcing and friction. The predictions of the perturbation analysis are verified numerically with computations of Poincaré sections for solutions in the stable and unstable manifolds of the hyperbolic periodic orbit and with computations of solutions for general initial-value problems. In the presence of constant positive wind stress τ_0 (equatorward on eastern ocean boundaries), chaotic solutions exist when the ratio of the oscillatory wind stress τ_1 to the bottom friction parameter r is above a critical value that depends on τ_0/r and the bottom topographic height. The analysis complements a previous study of this model (Samelson & Allen 1987), in which chaotic solutions were observed numerically for weak near-resonant forcing and weak friction.

1. Introduction

A nearly universal characteristic of mesoscale currents in the coastal ocean is the complexity of their time dependence (e.g. Allen 1980). Most coastal ocean velocity fields, as observed from moored current meters with limited temporal resolution,

contain energy in an apparently continuous (often red, sometimes peaked) band of frequencies below the local inertial frequency. This is presumably due in part to the wide range of frequencies and scales at which the coastal ocean is forced, and in part to instabilities and nonlinearities of the flow field that transfer energy between frequencies. The unpredictable nature of the atmospheric circulation in response to essentially periodic forcing by solar radiation has led to the consideration of atmospheric models in which instabilities and nonlinearities give rise to irregular, 'chaotic' time evolution (Lorenz 1963, 1984). The postulation of a chaotic mechanism to explain irregularity in coastal currents has evidently seemed unnecessary, perhaps in part because the velocity fields over most continental shelves are themselves forced by complex and rapidly evolving meteorological conditions.

Recent research has resulted, however, in the discovery of chaos in theoretical and laboratory models of a number of geophysical fluid dynamical processes relevant to the coastal ocean. These include models of baroclinic instability (Pedlosky & Frenzen 1980; Pedlosky 1981*a*, *b*; Klein & Pedlosky 1986; Hart 1985, 1986; Ohlsen & Hart 1989), internal waves (Abarbanel 1983), and forced flow over topography (Samelson & Allen 1987). Whether this discovery will lead to new and useful insights into the dynamics of coastal currents is a question of considerable interest that will require continued theoretical and observational efforts to resolve. Here, we present further analysis of chaotic behaviour in the model of forced flow over topography originally developed to study mean flow generation by Samelson & Allen (1987). (In that study, attention was restricted to weak near-resonant forcing with zero time-mean, and chaotic numerical solutions were found for certain parameter values.) We investigate the effect of weak forcing that is time-periodic at arbitrary frequency and has a constant component. We have two goals: to provide an analytical demonstration of the existence of chaotic solutions of a systematically derived (albeit highly idealized) model of coastal currents, and to improve understanding of the manner in which chaos arises in this particular model.

2. Model equations

The governing equations have been derived as a simple model for flow over the continental margin by Samelson & Allen (1987), who investigated mean flow generation by topographic interaction. We briefly review that derivation here.

The coastal ocean over the continental shelf and slope is represented in the model by a single layer of homogeneous fluid that obeys the quasi-geostrophic potential vorticity equation (Pedlosky 1987). The fluid is contained between channel walls at the coast and the deep ocean, and forced by an alongshore (along-channel) wind stress that is uniform in space but may vary in time. The bottom topography consists of a uniform offshore slope plus sinusoidal alongshore corrugations that vanish at the channel walls. Figure 1 shows the model geometry schematically. Right-handed Cartesian coordinates are chosen with y' positive onshore, z' positive upward, and x' positive in the direction opposite to topographic Rossby wave phase propagation.

Dependent and independent variables are non-dimensionalized as follows. The dimensionless stream function $\psi = p'/\rho U_0 fL$, coordinates $(x, y) = (x', y')/L$, time $t = t' U_0/L$, bottom topography $h = h'/R_0 D$, friction $\hat{r} = \delta_E/2R_0 D$, and wind stress $\hat{\tau}^x = \tau'/\tau_*$. Primes denote dimensional variables, and p' is pressure. The density ρ, Coriolis parameter f, velocity, length, and depth scales U_0, L, and D, bottom Ekman layer depth δ_E, and wind stress scale $\tau_* = \rho U_0 f R_0 D = \rho U_0^2 D/L$ are dimensional constants, and $R_0 = U_0/fL$ is the Rossby number. The velocity U_0 is taken to be the

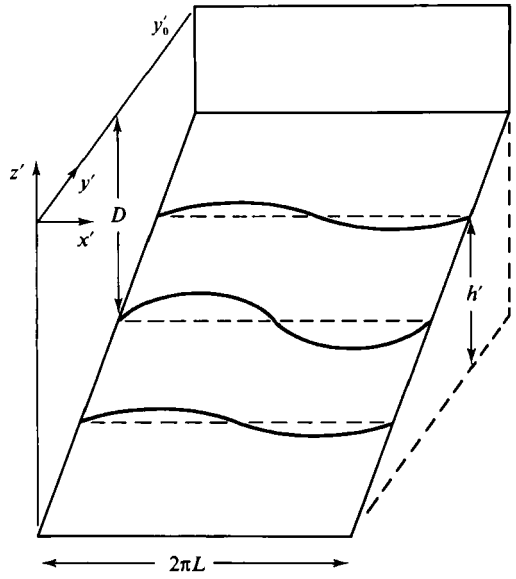

FIGURE 1. Schematic of model geometry. The idealized case considered involves the assumption $2\pi L \ll y'_0$.

fundamental scale, and the lengthscale L is chosen by setting $L^2 = U_0 D/f(\mathrm{d}h'/\mathrm{d}y')$, so that $2\pi L$ turns out to be the wavelength of a resonant topographic wave when the alongshore flow is equal to U_0.

Following Hart (1979), Samelson & Allen (1987) consider bottom corrugations whose alongshore (along-channel) wavelength is short relative to the scale of their cross-shelf (cross-channel) variations. Then the topography may be written

$$h(x, y) = y + \sqrt{2}\delta \cos x, \tag{2.1}$$

where the amplitude δ of the corrugations may vary only slowly in y, and the non-dimensional quasi-geostrophic stream function may be decomposed as

$$\psi(x, y, t) = -U(t)\, y + \phi(x, t), \tag{2.2}$$

where U is the basic alongshore flow and ϕ is a stream function for motions due to the topography. An equation for U may be obtained by x-averaging the alongshore momentum equation over a wavelength of the corrugations. A simplified potential vorticity equation follows from the decomposition (2.2). The result is the coupled pair of equations

$$\frac{\mathrm{d}U}{\mathrm{d}t} = -\hat{r}U + \langle \phi_x h \rangle + \hat{\tau}^x, \tag{2.3a}$$

$$\phi_{xxt} = -U\phi_{xxx} - \hat{r}\phi_{xx} - \phi_x - Uh_x, \tag{2.3b}$$

where

$$\langle \phi_x h \rangle = \frac{1}{2\pi} \int_x^{x+2\pi} \phi_x h \, \mathrm{d}x' = -\langle \phi h_x \rangle, \tag{2.4}$$

is the x-averaged wave drag (pressure force on the topography). In (2.3a), the acceleration $\mathrm{d}U/\mathrm{d}t$ of the alongshore flow is balanced by friction, x-averaged wave drag, and wind stress. In (2.3b), the rate of change ϕ_{xxt} of vorticity is balanced by alongshore advection, friction, and vortex stretching. There are two vortex-stretching terms: the first represents offshore flow over the shelf bottom slope, the

second alongshore flow over the topographic corrugations. For the present analysis, the forcing and friction will be small, and the forcing may contain a time-periodic part:

$$\hat{\tau}^x = \hat{\tau}_0 + \hat{\tau}_1 \cos \omega t = \epsilon(\tau_0 + \tau_1 \cos \omega t), \tag{2.5a}$$

$$\hat{r} = \epsilon r, \tag{2.5b}$$

where $0 < \epsilon \ll 1$. Equations equivalent to (2.3) were first derived and studied for steady forcing by Hart (1979). (Charney & DeVore 1979 obtained similar equations by spectral truncation.) Note that except for alongshore advection, the nonlinear terms have vanished in (2.3b), because of the anisotropy in the topography. The stream function ϕ has not been restricted to small amplitude.

Equations (2.3) may be reduced to a set of ordinary differential equations by substitution of the Fourier expansion

$$\phi = \sqrt{2}(\phi_1 \cos x + \phi_2 \sin x), \tag{2.6}$$

where ϕ_1 is in phase with topography (2.1) and ϕ_2 is out of phase. The result is

$$\frac{\mathrm{d}U}{\mathrm{d}t} = \delta\phi_2 + \epsilon(-rU + \tau_0 + \tau_1 \cos \omega t), \tag{2.7a}$$

$$\frac{\mathrm{d}\phi_1}{\mathrm{d}t} = -(U-1)\,\phi_2 + \epsilon(-r\phi_1), \tag{2.7b}$$

$$\frac{\mathrm{d}\phi_2}{\mathrm{d}t} = (U-1)\,\phi_1 - \delta U + \epsilon(-r\phi_2). \tag{2.7c}$$

In the absence of forcing and friction ($\hat{\tau}^x = \hat{r} = 0$), two conservation statements exist for (2.3) (Samelson & Allen 1987). The first expresses conservation of x-averaged kinetic energy, while the second results from the x-averaged potential enstrophy and alongshore momentum equations. For (2.7) with $\epsilon = 0$, the corresponding conserved quantities are

$$E = \tfrac{1}{2}(U^2 + \phi_1^2 + \phi_2^2), \tag{2.8a}$$

and

$$M = \tfrac{1}{2}(\phi_1^2 + \phi_2^2) - \delta\phi_1 + U, \tag{2.8b}$$

respectively.

For analysis of the forced damped system, (2.7) with $\epsilon > 0$, it is convenient to replace the 'in-phase' wave amplitude ϕ_1 with a new variable G formed from the difference of E and M, and to rewrite (2.7) as

$$\frac{\mathrm{d}U}{\mathrm{d}t} = F + \epsilon(-rU + \tau_0 + \tau_1 \cos \omega t), \tag{2.9a}$$

$$\frac{\mathrm{d}F}{\mathrm{d}t} = -G - (\omega_0^2 - G)\,U + \tfrac{3}{2}U^2 - \tfrac{1}{2}U^3 + \epsilon(-rF), \tag{2.9b}$$

$$\frac{\mathrm{d}G}{\mathrm{d}t} = \epsilon[-rG - \tfrac{1}{2}rU^2 + (U-1)(\tau_0 + \tau_1 \cos \omega t)], \tag{2.9c}$$

where

$$F = \delta\phi_2, \tag{2.10a}$$

$$G = E - M = \tfrac{1}{2}U^2 - U + \delta\phi_1, \tag{2.10b}$$

and

$$\omega_0^2 = 1 + \delta^2. \tag{2.11}$$

The in-phase wave amplitude ϕ_1 may be retrieved from G using (2.10b),

$$\phi_1 = \frac{G - \frac{1}{2}U^2 + U}{\delta}. \tag{2.12}$$

The system (2.9) with $\epsilon = 0$ is Hamiltonian, with canonical coordinates U and F and Hamiltonian function

$$\begin{aligned}\hat{H}(U,F) = \hat{H}(U,F;G) &= \tfrac{1}{2}F^2 + GU + \tfrac{1}{2}(\omega_0^2 - G)\,U^2 - \tfrac{1}{2}U^3 + \tfrac{1}{8}U^4, \\ &= \delta^2 E - \tfrac{1}{2}G^2,\end{aligned} \tag{2.13}$$

so that (2.9) may be rewritten as

$$\frac{\mathrm{d}U}{\mathrm{d}t} = \frac{\partial \hat{H}}{\partial F} + \epsilon g_1, \tag{2.14a}$$

$$\frac{\mathrm{d}F}{\mathrm{d}t} = -\frac{\partial \hat{H}}{\partial U} + \epsilon g_2, \tag{2.14b}$$

$$\frac{\mathrm{d}G}{\mathrm{d}t} = \epsilon g_3, \tag{2.14c}$$

where

$$g_1 = -rU + \tau_0 + \tau_1 \cos \omega t, \quad g_2 = -rF, \tag{2.15a, b}$$

$$g_3 = -rG - \tfrac{1}{2}rU^2 + (U-1)(\tau_0 + \tau_1 \cos \omega t). \tag{2.15c}$$

The Hamiltonian system (2.13) with $\epsilon = 0$ describes the natural oscillations (free waves) of alongshore flow and potential vorticity that occur in the model in the absence of friction and forcing. The energy–enstrophy quantity G appears only as a parameter when $\epsilon = 0$.

Choices for magnitudes of the characteristic dimensional variables used in the non-dimensionalization so that the model corresponds approximately to flow fields over the upper continental slope are discussed in Samelson & Allen (1987). The values assumed there are $U_0 = 10$ cm s^{-1}, $D = 250$ m, $\mathrm{d}h'/\mathrm{d}y' = 10^{-2}$, and $f = 10^{-4}$ s^{-1}. This implies $L = 5$ km ($2\pi L \approx 30$ km) and $R_0 = 0.2$. The dimensional $\delta' = R_0 D \delta$, where $R_0 D = 50$ m, so $\delta = O(1)$ is appropriate. The timescale $L/U_0 \approx 0.6$ days so the dimensional period of the forcing $2\pi L/\omega U_0$ is about $4/\omega$ days and we consider $\omega = O(1)$. For a dimensional alongshore wind stress $\tau_\mathrm{p} = 1$ dyn cm^{-2} and a bottom Ekman layer depth of $\delta_\mathrm{E} = 10$ m (corresponding to a dimensional frictional timescale of $T_F = 2D/(\delta_\mathrm{e} f) \approx 6$ days) the resulting magnitudes of the dimensionless wind stress and friction parameters are $\hat{\tau}^x = \tau_\mathrm{p}/\tau_* = 0.2$ and $\hat{r} = 0.1$. In the analysis, we take advantage of the small values indicated for $\hat{\tau}^x$ and $\hat{r}$ and consider the limit of weak forcing and friction. The results depend on the dimensionless parameters $\hat{\tau}/\hat{r} = 2\tau_\mathrm{p}/(\rho U_0 f \delta_\mathrm{E})$, $\delta = \delta'/R_0 D$, and $\omega = 2\pi L/U_0 T_\mathrm{p}$, where T_p is the dimensional period of the forcing. The model is clearly highly idealized, but it includes several of the basic physical processes of continental slope flow fields in a reasonable and relatively simple way. Our object is the investigation of possible qualitative features of the nonlinear response of wind-forced flow over the continental slope and not the precise prediction of the magnitude or structure of oceanic velocity fields.

3. Free waves and steady damped response

Since the response to time-variable forcing ($\epsilon > 0, \tau_1 \neq 0$) that is weak ($\epsilon \ll 1$) will depend importantly on the dynamics that govern the flow when the forcing is absent or time-independent, it is useful to review the properties of the free waves ($\epsilon = 0$) and

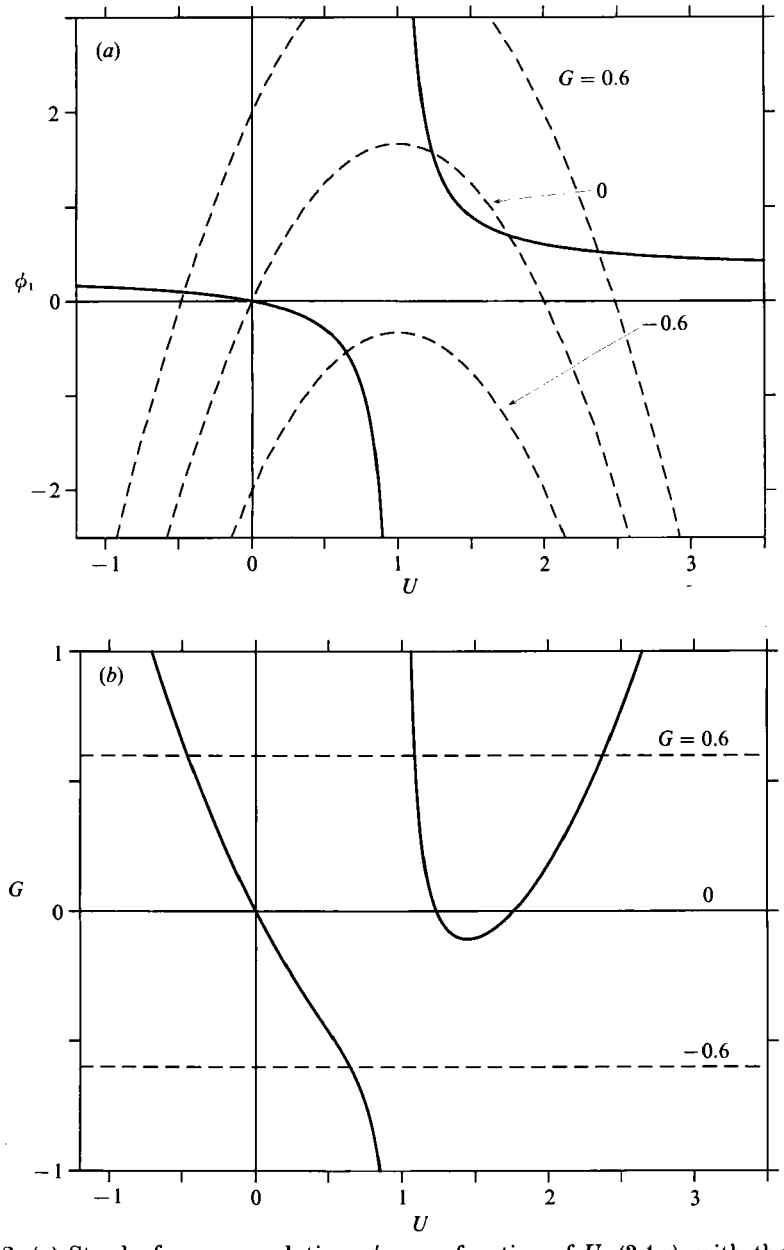

FIGURE 2. (*a*) Steady free-wave solutions ϕ_1 as a function of U, (3.1*a*), with three contours of constant G from (3.2) shown. (*b*) Steady free-wave solutions G as a function of U, (3.2), with lines drawn at the constant-G values shown in (*a*). ($\delta = 0.3003$ in both (*a*) and (*b*).)

the frictional response to steady forcing ($\epsilon > 0, \tau_0 \neq 0, \tau_1 = 0$). Some of these solutions of (2.7) have been previously studied by Hart (1979), Charney & DeVore (1979), and Samelson & Allen (1987).

3.1. *Free waves*

Consider first the steady free-wave solutions of (2.7) with $\epsilon = 0$. They satisfy

$$\phi_1 = \frac{\delta U}{U-1}, \quad \phi_2 = 0, \tag{3.1a, b}$$

for arbitrary U, provided $U \neq 1$. Vorticity produced by alongshore flow over the corrugations is balanced by alongshore advection of relative vorticity and vortex stretching by cross-shelf motion over the slope. No vorticity out of phase with the topography exists, so there is no wave drag on the alongshore flow. A resonance occurs when $U = 1$, i.e. when the alongshore flow is equal in magnitude to the oppositely directed phase velocity of the free topographic Rossby waves with x variability given by (2.6). Figure 2(*a*) shows a graph of ϕ_1 versus U for the solution (3.1*a*). Far from the resonance $U = 1$, the wave amplitude ϕ_1 approaches the corrugation amplitude δ. Near the resonance, ϕ_1 approaches infinity, changing sign across the resonance. The linear stability of these waves may be determined from the eigenvalues of the linearization of (2.7) at (3.1). They are neutrally stable (zero eigenvalue) to perturbations along the solution curve (3.1), since such perturbations simply transform one steady free wave into another and excite no time-dependent response. For other perturbations, they are neutrally stable (two non-zero imaginary eigenvalues) for $U < 1$ and for $U > 1+\delta^{\frac{2}{3}}$, and unstable (one positive and one negative eigenvalue) for $1 < U < \delta^{\frac{2}{3}}$.

The unperturbed ($\epsilon = 0$) system (2.7) may be integrated in terms of elliptic functions (Charney & DeVore 1979), as is evident from the Hamiltonian representation (2.13), so a complete description of all linear and nonlinear free-wave solutions may be found. The energy–enstrophy quantity G is conserved by both steady and unsteady free waves, and appears as a parameter in the Hamiltonian (2.13). Figure 2(*a*) shows selected lines of constant G overlaid on the graph of the steady free-wave solutions. Figure 2(*b*) is a similar plot with G as the ordinate, where from (2.10*b*) and (3.1*a*), the steady solutions are given by

$$G = \frac{U(U^2-3U+2\omega_0^2)}{2(U-1)}. \tag{3.2}$$

Note that while for each ϕ_1 there is a single value of alongshore flow U yielding a steady solution, for a given G there may be either one, two, or three values of U yielding steady solutions.

An equation for the steady solutions U in terms of G may be found from (3.2) or from (2.9*b*) with $\mathrm{d}F/\mathrm{d}t = 0$. The result is

$$U^3-3U^2+2(\omega_0^2-G)\,U+2G = 0, \tag{3.3}$$

which has one real root for $G < G_c$, two for $G = G_c$, and three for $G > G_c$, where

$$G_c = \tfrac{3}{2}\delta^{\frac{4}{3}}+\delta^2-\tfrac{1}{2}. \tag{3.4}$$

The unsteady free waves are restricted to move on lines of constant G in figure 2, since they conserve G, but to describe the time-dependent motion the plots must be supplemented with the scaled out-of-phase wave amplitude F. Figure 3 shows contours of $\hat{H}(U, F; G)$ for two values of G. $\hat{H}$ is also conserved by the free waves, so the unsteady free-wave solutions must follow contours of $\hat{H}$ as they evolve in time. The steady free-wave solutions (3.1) or (3.3) are marked. In figure 3(*a*), $G < G_c$ and

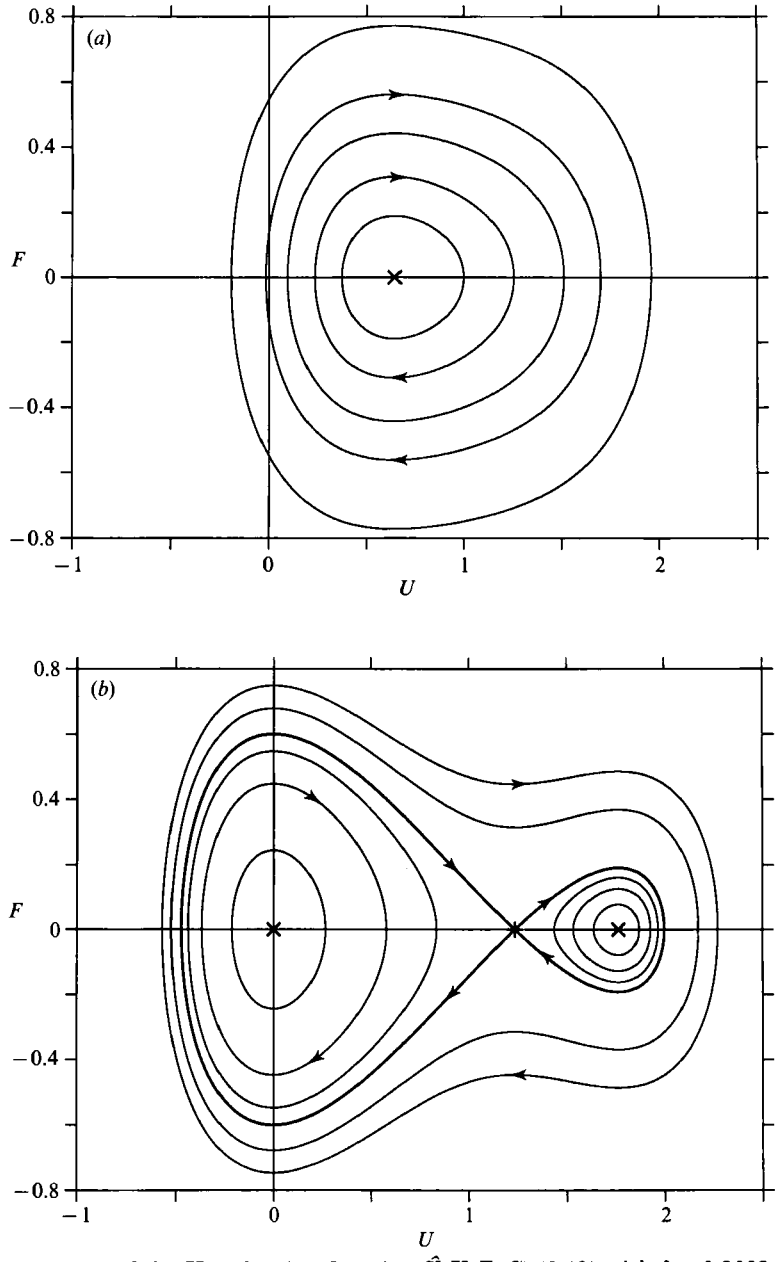

FIGURE 3. Contours of the Hamiltonian function $\hat{H}(U,F;G)$ (2.13) with $\delta = 0.3003$ for two of the values of G that are shown in figure 2. The steady solutions, $F = 0$ and U from (3.3), are marked. (*a*) $G = -0.6$, (*b*) $G = 0$.

there is a single steady state (an elliptic centre), while in figure 3(*b*), $G > G_c$ and there are three possible steady states (two elliptic centres and a saddle point).

By (2.9*a*) with $\epsilon = 0$, the time evolution of the unsteady free waves is clockwise along the contours, as the direction of the pressure force (2.4) on the alongshore flow depends only on the sign of $\phi_2 = F/\delta$. In figure 3(*a*), the unsteady waves are all periodic oscillations around the single steady wave. The alongshore flow U is alternately stronger and weaker than for the steady wave, and the out-of-phase wave

ϕ_2 oscillates around zero in quadrature with U. In figure 3(*b*), there are three steady waves, and three classes of unsteady waves. The first class of unsteady waves consists of oscillations around the steady wave with strong alongshore flow, and the second consists of oscillations around the steady wave with zero alongshore flow. These are represented by the contours inside the right and left lobes, respectively, of the separatrix, the 'figure-eight' contour that passes through the steady wave with intermediate alongshore flow. The third class of oscillations consists of large-amplitude free waves that oscillate around all three steady waves, following contours outside the separatrix. The separatrix waves for each lobe are mathematically similar to the motion of a pendulum which asymptotically approaches its (unstable) upright position. In that case, the separatrix separates the classes of oscillations for which the pendulum rod circles its support from those for which it swings back and forth.

The separatrix itself consists of the unstable steady wave and two (nonlinear) unsteady free waves, which do not oscillate but rather asymptotically approach the unstable steady wave in both forward and backward time. Solutions for the separatrix waves may be found analytically. For

$$G = G_s > G_c \tag{3.5a}$$

let

$$U = U_s \tag{3.5b}$$

be the intermediate root (saddle point) of (3.3) corresponding to the unstable steady wave. For $\epsilon = 0$ we define

$$U = U_0 = U_s + V_0, \quad F = F_0, \quad G = G_s, \tag{3.6a, b, c}$$

so that (2.14) are

$$\frac{dV_0}{dt} = \frac{\partial H_0}{\partial F_0} = F_0, \tag{3.7a}$$

$$\frac{dF_0}{dt} = -\frac{\partial H_0}{\partial V_0} = k^2 V_0 - \tfrac{3}{2}(U_s - 1)\, V_0^2 - \tfrac{1}{2} V_0^3, \tag{3.7b}$$

where

$$H_0 = \tfrac{1}{2}F_0^2 - \tfrac{1}{2}k^2 V_0^2 + \tfrac{1}{2}(U_s - 1)\, V_0^3 + \tfrac{1}{8}V_0^4, \tag{3.7c}$$

and

$$k^2 = G_s - \omega_0^2 + 3U_s - \tfrac{3}{2}U_s^2 > 0. \tag{3.7d}$$

That $k^2 > 0$ follows from (3.3), (3.4) and (3.5), with the intermediate deduction that $1 < U_s < 1 + \delta^{\frac{2}{3}}$. As a result of (3.6) and the definition of U_s (3.5b), $H_0 = 0$ on the separatrix so that (3.7*a*, *c*) imply

$$\frac{dV_0}{dt} = \pm \tfrac{1}{2} V_0 [4k^2 - bV_0 - V_0^2]^{\frac{1}{2}}, \tag{3.8a}$$

where

$$b = 4(U_s - 1) > 0. \tag{3.8b}$$

The solution of (3.8*a*) is

$$V_0(t - t_0) = V_{0\pm}(t - t_0) = \frac{8k^2 V_{m\pm}}{bV_{m\pm} + (8k^2 - bV_{m\pm}) \cosh[k(t - t_0)]}, \tag{3.9a}$$

where

$$V_{m\pm} = \tfrac{1}{2}[-b \pm (b^2 + 16k^2)^{\frac{1}{2}}]. \tag{3.9b}$$

The separatrix solutions for $F_0(t - t_0)$ may be found from (3.7*a*). The solutions (3.9) have been chosen so that, at $t = t_0$, $F_0(0) = 0$, and $U_0(0) = U_s + V_{m\pm}$, the maximum (+) or minimum (−) values of the alongshore flow attained for the separatrix waves.

For $t \to \pm\infty$, the separatrix waves approach the unstable (saddle point) steady wave $(U_s, 0, G_s)$ and obey the linearized forms of (3.7a, b),

$$\frac{dV_0'}{dt} = F_0', \quad \frac{dF_0'}{dt} = k^2 V_0', \tag{3.10}$$

so that the saddle-point eigenvalues are $\pm k$, and the corresponding stable and unstable linear modes are

$$(U, F) = (U_s, 0) + (1, -k)\hat{A}^s \exp[-k(t-t_1)], \tag{3.11a}$$

and

$$(U, F) = (U_s, 0) + (1, k)\hat{A}^u \exp[k(t-t_2)], \tag{3.11b}$$

where, from the limit of (3.9) as $t \to \pm\infty$,

$$\hat{A}^s = V_{L\pm} \exp[-k(t_1 - t_0)], \quad \hat{A}^u = V_{L\pm} \exp[k(t_2 - t_0)], \tag{3.11c, d}$$

$$V_{L\pm} = \frac{16k^2 V_{m\pm}}{(8k^2 - bV_{m\pm})}. \tag{3.11e}$$

Thus, inviscid free waves near the unstable steady free wave will approach it if $\delta\phi_2 \approx -k(U-U_s)$ and depart from it if $\delta\phi_2 \approx k(U-U_s)$. At finite amplitude, the separatrix waves link the opposite-stability linear modes of the steady free wave, and 'separate' the three oscillatory regimes. In §4, the special character of the separatrix waves is exploited to investigate the conditions under which the flow can become chaotic in the presence of weak time-dependent forcing and weak friction.

3.2. *Steady frictional response*

The steady frictional response ($\epsilon > 0, \tau_0 \neq 0, r \neq 0, \tau_1 = 0$) of (2.7) has been studied by Hart (1979) and Charney & DeVore (1979). Setting time derivatives equal to zero in (2.7) or (2.9) yields a cubic equation for the alongshore flow U,

$$U^3 - \left(2 + \frac{\tau_0}{r}\right) U^2 + \left(\omega_0^2 + \epsilon^2 r^2 + \frac{2\tau_0}{r}\right) U - (1 + \epsilon^2 r^2)\frac{\tau_0}{r} = 0, \tag{3.12a}$$

and

$$F = \epsilon(rU - \tau_0), \tag{3.12b}$$

$$G = (U-1)\frac{\tau_0}{r} - \tfrac{1}{2}U^2. \tag{3.12c}$$

Equation (3.12a) may be rewritten

$$\frac{\tau_0}{r} = P(U), \tag{3.13a}$$

where

$$P(U) = U + \frac{\delta^2 U}{(U-1)^2 + \epsilon^2 r^2}, \tag{3.13b}$$

and solved graphically for given δ and ϵr, as illustrated in figure 4. For small or large τ_0/r, there is a single steady response, while for intermediate values of τ_0/r, three steady responses are possible as illustrated by the dashed line in figure 4 at one value of $P(U) = \tau_0/r$. The linear stability of these solutions can be shown to depend on the sign of dP/dU, so that the intermediate of the three steady responses with $dP/dU < 0$ is unstable (when it exists), while the others are stable (unless $dP/dU = 0$, for which unusual case they are neutral). For weak forcing and friction ($\epsilon \ll 1$), the steady response for F is order ϵ by (3.12b), so by (2.9b) the cubic equation (3.12a) for U differs from (3.3) by only order ϵ^2, and the steady forced solutions to (3.12) will be close to steady free-wave solutions of (3.3) when the respective values

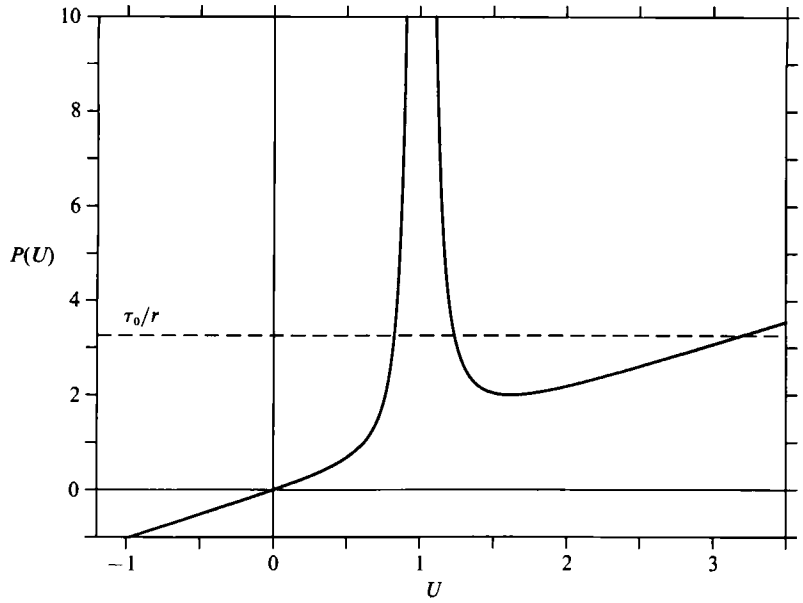

FIGURE 4. Steady frictional response given by $\tau_0/r = P(U)$, (3.13), for $\delta = 0.3003$ and $\epsilon r = 10^{-4}$. The solid line is $P(U)$ while the dashed line is $\tau_0/r = 3.236$. The intersections of the solid and dashed lines give the values of U corresponding to the three steady solutions of (3.12*a*) at this value of τ_0/r. The intermediate solution with $dP/dU < 0$ is linearly unstable. These values of δ and τ_0/r are used in the numerical solutions in §6.

of G coincide. For the forced solutions, G is determined by (3.12*c*), and in general will have three different values for the three steady responses.

4. The Melnikov criterion

For weak steady plus time-periodic forcing ($0 < \epsilon \ll 1, \tau_0 \neq 0, \tau_1 \neq 0$), chaotic behaviour can occur in the model in which the flow switches randomly between the three oscillatory free-wave regimes. The existence of this irregular response to regular forcing is associated with the occurrence of Smale horseshoes (Smale 1963, 1967; Guckenheimer & Holmes 1983) in the model dynamics. The occurrence of such horseshoes is demonstrated analytically in this section, following an extension (Wiggins & Holmes 1987) of the method of Melnikov (1963).

Melnikov's method is an analytical technique developed to determine how separatrix solutions behave under perturbation. It yields a criterion for the existence in the perturbed system of a transverse 'homoclinic orbit', that is, a solution that is asymptotic to the same state in both forward and backward time. (The separatrix solutions of the unperturbed system are themselves non-transverse homoclinic orbits.) When combined with the Smale–Birkhoff homoclinic theorem (Smale 1963), this criterion may be used to prove the existence of chaotic solutions of the perturbed equations (Guckenheimer & Holmes 1983). This approach is one of the very few analytical techniques currently available for rigorously demonstrating the existence of chaotic solutions of a set of differential equations (Wiggins 1988).

In the model considered here, the satisfaction of the Melnikov criterion is (essentially) equivalent to the following conditions: (i) for some value of the

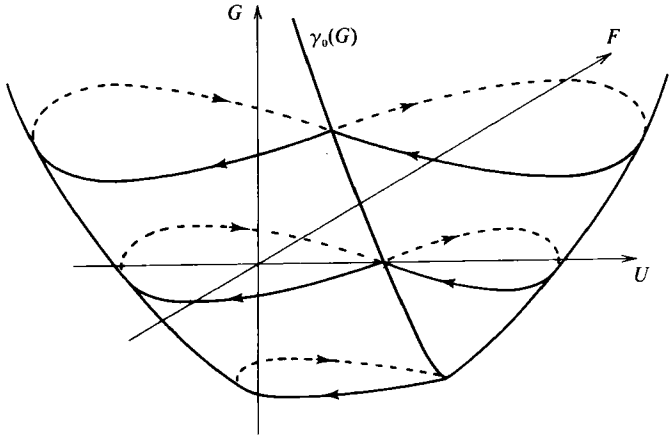

FIGURE 5. Schematic of the phase-space structure of the unperturbed system (2.14) with $\epsilon = 0$ for fixed δ (e.g. $\delta \approx 0.3$) showing the one-dimensional manifold $\gamma_0(G)$ and the surface of separatrices containing both the stable manifold W_0^s and the unstable manifold W_0^u of γ_0.

energy–enstrophy quantity G, an unstable steady free wave 'survives' the perturbation (weak forcing and damping) as an unstable periodic small-amplitude oscillation at the forcing frequency; (ii) for a particular phase of the forcing relative to the wave, a separatrix free wave 'survives' the perturbation as a forced wave that is asymptotic to the periodic oscillation in both forward and backward time. Under these conditions, forced waves near the 'surviving' separatrix wave will be chaotic. That this should be so is not intuitively obvious. We do not repeat the argument here, since it has been carried out fully elsewhere and requires considerable technical detail. The chaotic behaviour is associated with the recurrent approach of the flow to states near the unstable oscillation. Geometric analysis reveals that when the Melnikov criterion is satisfied, this recurrence generates invariant Cantor sets of solutions, whose behaviour may be related to shift maps operating on infinite sequences of binary digits. For further discussion of the connection between the Melnikov criterion and the chaotic solutions, we refer the reader to Guckenheimer & Holmes (1983) and Wiggins (1988). A description of the nature of the chaotic dynamics that occurs specifically in the case of three variables is given by Wiggins & Shaw (1988). While it is not simple to unravel the physical interpretation of these analyses, it is worth noting that chaotic behaviour has often been associated with the recurrent approach of systems to unstable states (Šilnikov 1965; Sparrow 1982). The linear instability causes the future evolution of the system to depend sensitively on its precise approach to the unstable state. Chaos may result if nonlinear effects conspire to alter that approach appropriately with each recurrence.

Some information about the behaviour of the perturbed system may be gained from the invariant manifold theory (Hirsch, Pugh & Shub 1977). The unstable steady wave solution (3.5) depends continuously on G by (3.3), and so may be represented by the continuous curve (one-dimensional manifold)

$$\gamma_0(G): \quad (U, F, G) = (U_s(G), 0, G) \tag{4.1}$$

of points in the (U, F, G) phase space. Similarly, the separatrix waves depend continuously on G and form a surface (two-dimensional manifold) of (U, F, G) points. The phase-space structure of the unperturbed system is shown schematically in figure 5. The surface of separatrices contains both the stable manifold W_0^s of γ_0 (the free waves asymptotic to the steady free waves in forward time) and the unstable

manifold W_0^u of γ_0 (the free waves asymptotic to the steady free waves in backward time), which are in this case the same. These manifolds are invariant: a solution with initial conditions in one of them remains within it forever. It follows from the perturbation results of the invariant manifold theory (Hirsch *et al.* 1977; Wiggins & Holmes 1987) that for sufficiently small ϵ there is an invariant manifold γ_ϵ within order ϵ of γ_0. This means that there is a set of forced waves γ_ϵ that remains forever close to the set of unstable steady free waves γ_0. Note that the closeness of γ_ϵ and γ_0 applies to the manifolds and not necessarily to individual solutions within them, so that a given forced wave may be close to different free waves at different times. (These conclusions apply as long as $G(t) > G_c$.)

To establish the existence of a periodic oscillation among the solutions in the invariant manifold γ_ϵ, it is necessary only to find a periodic solution of (2.9*c*) on γ_0 (since G parameterizes γ_0 and $|\gamma_\epsilon - \gamma_0| = O(\epsilon)$). This may be done (Wiggins & Holmes 1987) by obtaining a steady solution (with definite stability) of the equation

$$\overline{g_3(\gamma_\epsilon)} = \frac{\omega}{2\pi}\int_t^{t+2\pi/\omega} g_3(\gamma_\epsilon)\,\mathrm{d}t' = 0, \tag{4.2}$$

which results from averaging (2.9*c*) or (2.14*c*) over a forcing period on the invariant manifold γ_ϵ. Since $|g_3(\gamma_\epsilon) - g_3(\gamma_0)| = O(\epsilon)$, $g_3(\gamma_\epsilon)$ may be replaced with $g_3(\gamma_0)$ in (4.2) and the result for the steady solution of (4.2) is

$$G_s = -\tfrac{1}{2}U_s^2 + (U_s - 1)\frac{\tau_0}{r}, \tag{4.3}$$

to leading order in ϵ. For given δ and τ_0/r, (4.3) and (3.3) are two coupled equations for U_s and G_s, where $G_s > G_c$ is required and U_s must be the intermediate root of (3.3). Since

$$\frac{\mathrm{d}}{\mathrm{d}G}\overline{g_3(\gamma_0)}\bigg|_{G=G_s} = \frac{\mathrm{d}}{\mathrm{d}G_s}\overline{g_3[U(G_s), 0, G_s]} = -(r+\alpha) < 0, \tag{4.4}$$

where

$$\begin{aligned}\alpha &= -r(U_s - \tau_0)(U_s - 1)/k^2 \\ &= r[k^2 + (U_s - 1)^2 + \delta^2]/k^2 > 0,\end{aligned} \tag{4.5}$$

it follows that the solution (4.3) is linearly stable to perturbations in the invariant manifold γ_ϵ.

Note that when (4.3) is substituted into (3.3), there results

$$U_s^3 - \left(2 + \frac{\tau_0}{r}\right)U_s^2 + \left(\omega_0^2 + \frac{2\tau_0}{r}\right)U_s - \frac{\tau_0}{r} = 0, \tag{4.6}$$

which to second order in ϵ is just the equation for the steady damped response (3.12*a*). The steady solution (4.3) of the averaged equation (4.2) corresponds to a periodic oscillation of (2.9) for sufficiently small ϵ. Thus, weak periodic forcing perturbs the unstable steady frictional response to an unstable periodic oscillation. The existence of this oscillation satisfies the first of the two above conditions of the Melnikov criterion. Values of U_s from (4.6) and G_s from (4.3) as functions of δ and τ_0/r are plotted in figure 6.

The second condition is satisfied when the existence of the 'surviving' separatrix wave is established. This is accomplished by a perturbation technique originally due to Melnikov (1963). By the averaging theorem (Hale 1969), the unstable periodic

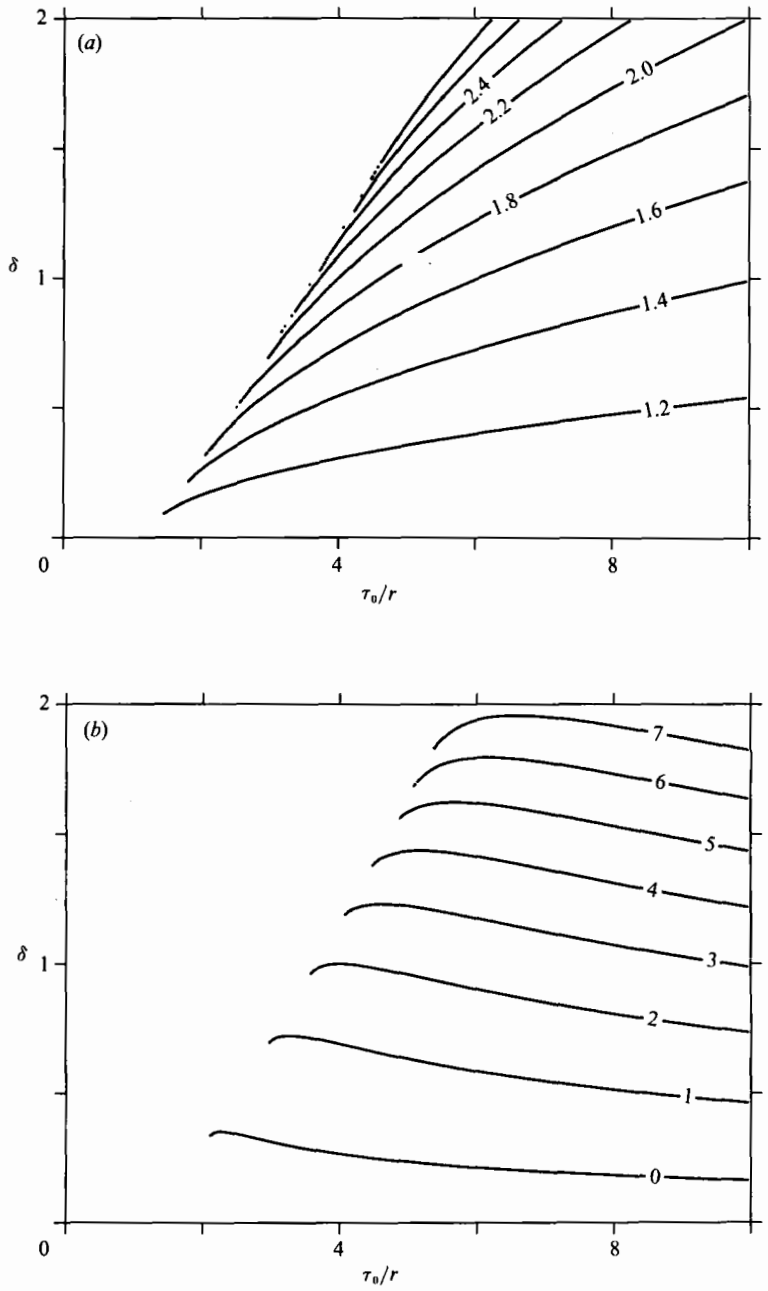

FIGURE 6. Contour plots of (*a*) U_s from (4.6) and (*b*) G_s from (4.3) as a function of τ_0/r and δ. These values give the location $(U, F, G) = (U_s, 0, G_s) + O(\epsilon)$ of the unstable periodic oscillations.

oscillation $p = \gamma_\epsilon(G_s) + O(\epsilon)$ of (2.9) is uniformly approximated to order ϵ for $t \in (-\infty, \infty)$ by the solution (4.3). The solutions asymptotic to p in forward time will be denoted $W^s_\epsilon(p)$, while those asymptotic to p in backward time will be denoted $W^u_\epsilon(p)$. The manifolds $W^s_0(\gamma_0)$, $W^u_0(\gamma_0)$, $W^s_\epsilon(p)$, $W^u_\epsilon(p)$ are shown schematically in figure 7. For the perturbed system, the manifolds are shown in a Poincaré section with time interval equal to the forcing period $2\pi/\omega$.

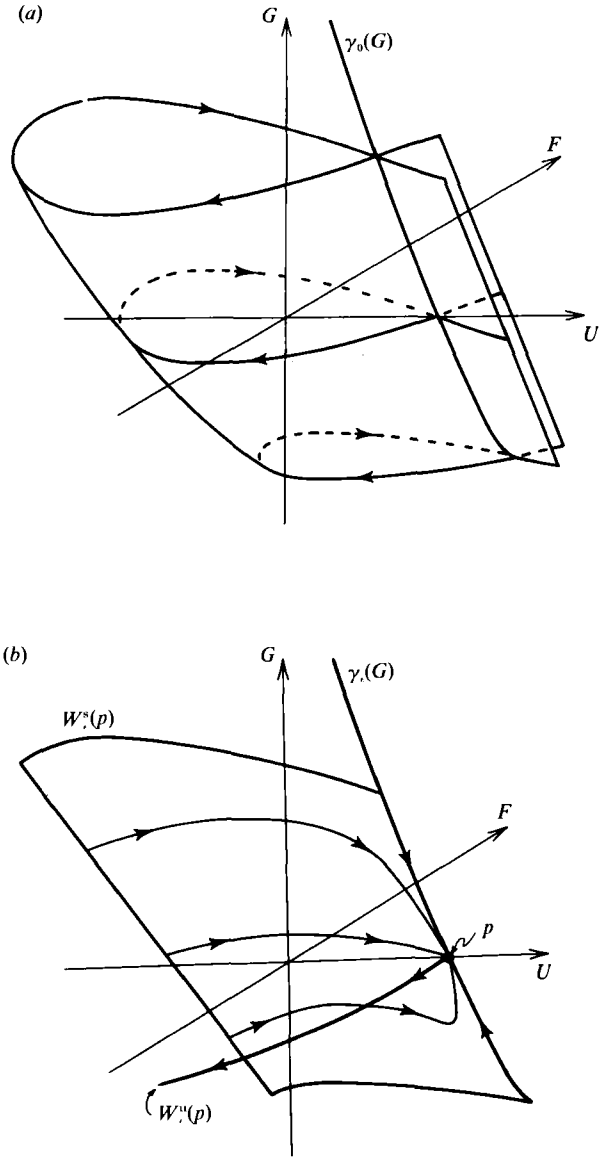

FIGURE 7. Schematic showing the change in geometry of the manifolds of the unperturbed system (2.14) with $\epsilon = 0$ under perturbation $0 < \epsilon \ll 1$. For clarity, only a part of the manifolds corresponding to the left lobe of the separatrices are shown. (*a*) A section of the unperturbed phase space as in figure 5. (*b*) A Poincaré section at time interval equal to the forcing period $2\pi/\omega$ showing the invariant manifold $\gamma_\epsilon(G)$ and also the two-dimensional stable manifold $W^s_\epsilon(p)$ and the one-dimensional unstable manifold $W^u_\epsilon(p)$ of the unstable periodic oscillation $p = \gamma_\epsilon(G_s) + O(\epsilon)$, where here $G_s = 0$.

We express the solutions $\boldsymbol{q}^s_\epsilon \in W^s_\epsilon(p)$ and $\boldsymbol{q}^u_\epsilon \in W^u_\epsilon(p)$ for semi-infinite time intervals as a separatrix wave plus perturbation terms as follows (Wiggins & Holmes 1987):

$$\boldsymbol{q}^s_\epsilon(t, t_0) = \boldsymbol{q}_0 + \epsilon \boldsymbol{q}^s_1 + O(\epsilon^2), \quad t \in [t_0, \infty), \tag{4.7a}$$

$$\boldsymbol{q}^u_\epsilon(t, t_0) = \boldsymbol{q}_0 + \epsilon \boldsymbol{q}^u_1 + O(\epsilon^2), \quad t \in (-\infty, t_0], \tag{4.7b}$$

where

$$\boldsymbol{q}_0(t - t_0) = (U_0, F_0, G_s), \tag{4.8}$$

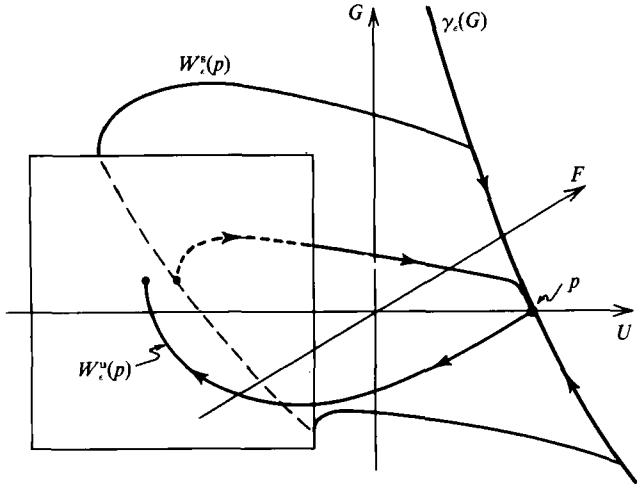

FIGURE 8. Schematic showing the geometry in a Poincaré section at time interval $2\pi/\omega$ of the solutions in $W^u_\epsilon(p)$ and $W^s_\epsilon(p)$ considered in the application of Melnikov's method. We consider $\boldsymbol{q}^{s,u}_\epsilon(t,t_0)$ that satisfy (4.11*a*, *b*). Thus, we look for intersections when $t = t_0$ in the (U,G)-plane at $F = 0$, where a specific solution in $W^s_\epsilon(p)$ is chosen by requiring that $G^s(t_0,t_0) = G^u(t_0,t_0)$. The parameter $t_0 \in [0, 2\pi/\omega]$ specifies the phase of the Poincaré section relative to the sinusoidal forcing (2.5*a*).

and where (see §5 and Appendix A)

$$\boldsymbol{q}^{s,u}_1(t,t_0) = (V^{s,u}_1, F^{s,u}_1, G^{s,u}_1). \tag{4.9}$$

If the exact solutions $\boldsymbol{q}^{s,u}_\epsilon$ could be obtained explicitly, then the existence of a 'surviving' separatrix wave would be indicated if it could be shown that

$$\boldsymbol{q}^s_\epsilon(t_0,t_0) = \boldsymbol{q}^u_\epsilon(t_0,t_0), \tag{4.10}$$

for some t_0. It is possible, however, following Melnikov (1963) and Wiggins & Holmes (1987), to test the condition (4.10) using only $\boldsymbol{q}_0$ without actually calculating the full solution $\boldsymbol{q}^{s,u}_\epsilon$ or the first-order part $\boldsymbol{q}^{s,u}_1$, (4.9). The proof depends on the existence of the representation (4.7), but explicit solutions are required only for the unperturbed separatrix wave (4.8), given in (3.9).

Consider $\boldsymbol{q}^{s,u}_\epsilon(t,t_0)$ that satisfy

$$F^s(t_0,t_0) = F^u(t_0,t_0) = 0, \tag{4.11a}$$

$$G^s(t_0,t_0) = G^u(t_0,t_0), \tag{4.11b}$$

which by (4.7) imply $F^s_1(t_0,t_0) = F^u_1(t_0,t_0) = 0$ and $G^s_1(t_0,t_0) = G^u_1(t_0,t_0)$. If also

$$U^s(t_0,t_0) = U^u(t_0,t_0), \tag{4.12}$$

then (4.10) would be satisfied. The corresponding geometry in a Poincaré section is shown schematically in figure 8. Note that here we look for the satisfaction of (4.10) on a fixed plane in a Poincaré section for variable values of the parameter $t_0 \in [0, 2\pi/\omega]$, where t_0 specifies the phase of the Poincaré section relative to the sinusoidal forcing (2.5*a*). This is similar to the approach taken by Guckenheimer & Holmes (1983) for the planar case and gives results equivalent to those obtained using the alternative method of Wiggins & Holmes (1987) where the phase of the Poincaré section is fixed while the location of the plane is varied (see e.g. the discussion in §4.5 of Guckenheimer & Holmes 1983). The application of the conditions (4.11*a*, *b*) to $F^{s,u}_1(t_0,t_0)$ and $G^{s,u}_1(t_0,t_0)$ is discussed further in Appendix A.

The equality (4.12), and hence (4.10), may be conveniently tested by deriving an approximate expression for the change in Hamiltonian function (2.13) along $\boldsymbol{q}_\epsilon^{\mathrm{s}}$ and $\boldsymbol{q}_\epsilon^{\mathrm{u}}$, and then showing that the Hamiltonian may be inverted locally for the velocity U. A similar procedure was used by Arnol'd (1964). The following analysis is simplified if in place of (2.13) we choose a Hamiltonian function as in (3.7c), i.e.

$$\begin{aligned} H(U,F;G) &= \hat{H}(U,F;G)-G[U_{\mathrm{s}}-\tfrac{1}{2}U_{\mathrm{s}}^2]-\hat{H}(U_{\mathrm{s}},0;0), \\ &= \tfrac{1}{2}F^2-\tfrac{1}{2}k^2V^2+\tfrac{1}{2}(U_{\mathrm{s}}-1)\,V^3+\tfrac{1}{8}V^4-(G-G_{\mathrm{s}})[(U_{\mathrm{s}}-1)\,V+\tfrac{1}{2}V^2], \end{aligned} \tag{4.13a}$$

where

$$U = U_{\mathrm{s}}+V, \tag{4.13b}$$

so that

$$H[\gamma_0(G_{\mathrm{s}})] = 0, \quad \nabla H[\gamma_0(G_{\mathrm{s}})] = 0, \tag{4.14a,b}$$

where

$$\nabla H = \left(\frac{\partial H}{\partial U}, \frac{\partial H}{\partial F}, \frac{\partial H}{\partial G}\right). \tag{4.15}$$

By (2.14) and (4.13),

$$\begin{aligned} \frac{\mathrm{d}H(\boldsymbol{q}_\epsilon^{\mathrm{s,u}})}{\mathrm{d}t} &= \nabla H(\boldsymbol{q}_\epsilon^{\mathrm{s,u}})\cdot\frac{\mathrm{d}\boldsymbol{q}_\epsilon^{\mathrm{s,u}}}{\mathrm{d}t}, \\ &= \epsilon\nabla H(\boldsymbol{q}_\epsilon^{\mathrm{s,u}})\cdot\boldsymbol{g}(\boldsymbol{q}_\epsilon^{\mathrm{s,u}},t), \end{aligned} \tag{4.16}$$

where $\boldsymbol{g} = (g_1, g_2, g_3)$. If we utilize (4.7) and expand

$$H(\boldsymbol{q}_\epsilon^{\mathrm{s,u}}) = H(\boldsymbol{q}_0)+\epsilon H_1^{\mathrm{s,u}}+O(\epsilon^2), \tag{4.17}$$

where

$$H_1^{\mathrm{s,u}} = \nabla H(\boldsymbol{q}_0)\cdot\boldsymbol{q}_1^{\mathrm{s,u}} = \frac{\partial H}{\partial U}(\boldsymbol{q}_0)\,V_1^{\mathrm{s,u}}+\frac{\partial H}{\partial F}(\boldsymbol{q}_0)\,F_1^{\mathrm{s,u}}+\frac{\partial H}{\partial G}(\boldsymbol{q}_0)\,G_1^{\mathrm{s,u}}, \tag{4.18a}$$

$$\frac{\partial H}{\partial U}(\boldsymbol{q}_0) = -k^2V_0+\tfrac{3}{2}(U_{\mathrm{s}}-1)\,V_0^2+\tfrac{1}{2}V_0^3, \tag{4.18b}$$

$$\frac{\partial H}{\partial F}(\boldsymbol{q}_0) = F_0, \tag{4.18c}$$

$$\frac{\partial H}{\partial G}(\boldsymbol{q}_0) = -(U_{\mathrm{s}}-1)\,V_0-\tfrac{1}{2}V_0^2, \tag{4.18d}$$

then (4.16) may be written

$$\frac{\mathrm{d}H_1^{\mathrm{s,u}}}{\mathrm{d}t} = \nabla H(\boldsymbol{q}_0)\cdot\boldsymbol{g}(\boldsymbol{q}_0,t), \tag{4.19}$$

accurate to first order in ϵ. Integration of (4.19) over $(-\infty, t_0]$ for H_1^{u} and over $[t_0,\infty)$ for H_1^{s} gives

$$H_1^{\mathrm{u}}(t_0,t_0)-H_1^{\mathrm{u}}(t_0,-\infty) = \int_{-\infty}^{t_0}\nabla H(\boldsymbol{q}_0)\cdot\boldsymbol{g}(\boldsymbol{q}_0,t)\,\mathrm{d}t, \tag{4.20a}$$

$$H_1^{\mathrm{s}}(t_0,\infty)-H_1^{\mathrm{s}}(t_0,t_0) = \int_{t_0}^{\infty}\nabla H(\boldsymbol{q}_0)\cdot\boldsymbol{g}(\boldsymbol{q}_0,t)\,\mathrm{d}t. \tag{4.20b}$$

From (4.18), $H_1^{\mathrm{s}}(t\to\infty)\to 0$ and $H_1^{\mathrm{u}}(t\to-\infty)\to 0$, so that (4.20$a,b$) may be added to obtain

$$\begin{aligned} \Delta H_1(t_0) &= H_1^{\mathrm{u}}(t_0,t_0)-H_1^{\mathrm{s}}(t_0,t_0) \\ &= [\boldsymbol{q}_1^{\mathrm{u}}(t_0,t_0)-\boldsymbol{q}_1^{\mathrm{s}}(t_0,t_0)]\cdot\nabla H(\boldsymbol{q}_0(t_0)) \\ &= \int_{-\infty}^{\infty}\nabla H(\boldsymbol{q}_0)\cdot\boldsymbol{g}(\boldsymbol{q}_0,t)\,\mathrm{d}t. \end{aligned} \tag{4.21}$$

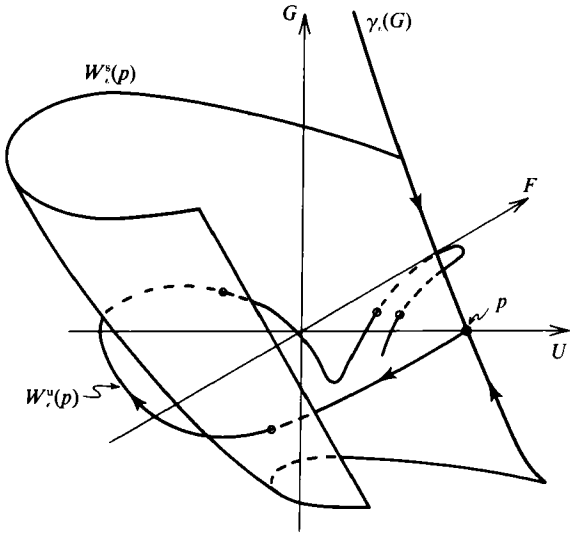

FIGURE 9. Schematic illustrating the intersection in a Poincaré section at time interval $2\pi/\omega$ of the two-dimensional stable manifold $W^s_\epsilon(p)$ and the one-dimensional unstable manifold $W^u_\epsilon(p)$, where here $G_s = 0$.

The $O(\epsilon)$ errors made in replacing $\nabla H(\boldsymbol{q}^{s,u}_\epsilon)\cdot\boldsymbol{g}(\boldsymbol{q}^{s,u}_\epsilon, t)$ with $\nabla H(\boldsymbol{q}_0)\cdot\boldsymbol{g}(\boldsymbol{q}_0, t)$ in (4.19) remain $O(\epsilon)$ in the integrals over infinite time in (4.20) and (4.21) because $\nabla H(\boldsymbol{q}_0)$ and its derivatives vanish exponentially as $t\to\pm\infty$. The quantity $\Delta H_1(t_0)$ is the first-order difference in Hamiltonian functions at $t = t_0$ for the solutions with $F^s(t_0, t_0) = F^u(t_0, t_0) = 0$ and $G^s(t_0, t_0) = G^u(t_0, t_0)$ that are asymptotic to the periodic oscillation p in forward and in backward time. If $\Delta H_1(t_0)$ has simple zeros, that is, if there exists a $t_0 = \tilde{t}_0$ such that

$$\Delta H_1(\tilde{t}_0) = 0, \tag{4.22a}$$

and if

$$\left.\frac{\mathrm{d}\Delta H_1(t_0)}{\mathrm{d}t_0}\right|_{t_0=\tilde{t}_0} \neq 0, \quad \frac{\partial}{\partial U}H[\boldsymbol{q}_0(\tilde{t}_0, \tilde{t}_0)] \neq 0, \tag{4.22b, c}$$

then it follows (Wiggins & Holmes 1987) from the implicit function theorem that $U^s(t_0, t_0) = U^u(t_0, t_0)$ for some t_0 near $\tilde{t}_0$, so (4.10) is satisfied and a homoclinic solution exists. Such a solution lies in both $W^s_\epsilon(p)$ and $W^u_\epsilon(p)$, and so constitutes an intersection of these manifolds. For a Poincaré section, the intersection is transverse if the zeros are simple so the hypotheses of the Smale–Birkhoff homoclinic theorem are satisfied. The condition (4.22*b*) is easily seen to be satisfied, since $\partial H/\partial U = -\mathrm{d}F/\mathrm{d}t$, and (4.22*a*) may be satisfied as discussed below. A schematic illustrating the resulting intersection of the manifolds is shown in figure 9. Note that with (4.14) the expression (4.21) agrees with (1) of Wiggins & Holmes (Errata, 1988), derived as the Melnikov function by alternative but similar means, since here

$$(\partial H/\partial G)[\gamma_0(G_s)] = 0.$$

Another derivation of the condition (4.22*a*) is presented in Appendix A, where it is obtained directly from the requirement that $U^s_1(t_0, t_0) = U^u_1(t_0, t_0)$.

The expression (4.21) may be evaluated using (4.18), (2.15) and (3.9). The result is

$$\Delta H_1(t_0) = rC_1 + \tau_1 C_2 \cos\omega t_0, \tag{4.23a}$$

where
$$C_1 = C_1^{\pm}\left(U_s - \frac{\tau_0}{r}\right)\left[8d\tan^{-1}\left(\frac{V_{m\pm}}{2k}\right) - kb\right], \tag{4.23b}$$

$$C_2 = C_2^{\pm} - 4\pi d\frac{\sinh\left[\omega\cos^{-1}(\alpha_{\pm})/k\right]}{\sinh(\omega\pi/k)}, \tag{4.23c}$$

$$d = k^2 + (U_s - 1)^2, \tag{4.23d}$$

$$\alpha_{\pm} = \frac{bV_{m\pm}}{(8k^2 - bV_{m\pm})}. \tag{4.23e}$$

Thus, $\Delta H_1(t_0)$ will have simple zeros provided

$$\frac{\tau_1}{r} > \left(\frac{\tau_1}{r}\right)_c^{\pm} = \left|\frac{C_1}{C_2}\right|, \tag{4.24}$$

where $(\tau_1/r)_c^{\pm}$ depends on τ_0/r and δ. Contours $(\tau_1/r)_c^{\pm}$ are plotted in figure 10 for $\omega = 1$ and $\omega = 0.5$. Instability increases as $(\tau_1/r)_c^{\pm}$ decreases, so as ω decreases. The chaotic invariant set that exists in (2.9) by (4.24) contains a countable infinity of unstable periodic oscillations of all periods that are integer multiples of the forcing period $2\pi/\omega$, an uncountable set of non-periodic oscillations, and an oscillation that approaches all others in the invariant set (a dense orbit). The periodic oscillations are all of saddle type and they are dense in the invariant set. Note that the chaotic set, while invariant, is not attracting. When both inequalities (+ and −) in (4.24) are satisfied, the set includes chaotic solutions for which the flow switches randomly between the three oscillatory free-wave regimes discussed in §3.1. Numerical calculations of solutions to (2.9) that verify the condition (4.24) and that illustrate the nature of the resulting chaotic solutions are presented in §6.

5. Approximate solutions for $G_1^{s,u}$

The Melnikov criterion (4.24) is verified by numerical calculation of solutions to (2.9) in $W_\epsilon^s(p)$ and $W_\epsilon^u(p)$ in §6. Because the intersection of the manifolds $W_\epsilon^s(p)$ and $W_\epsilon^u(p)$ indicated by (4.22*a*) occurs in a three-dimensional Poincaré section, as illustrated in figure 9, the situation is more complicated than for the planar two-variable case described, for example, in Guckenheimer & Holmes (1983). The implementation of appropriate numerical calculations in the present case requires the derivation of some additional results that concern approximate solutions for $G_1^{s,u}$.

Approximate linear solutions in $W_\epsilon^s(p)$ and $W_\epsilon^u(p)$ near the unstable periodic oscillation p are obtained in Appendix B. The resulting linear approximations to solutions in $W_\epsilon^s(p)$ for $t \in [t_1, \infty)$ are

$$U^s = U_s + \epsilon\left[A^s\exp\left[-k(t-t_1)\right] - \frac{(U_s-1)}{k^2}B\exp\left[-\epsilon(r+\alpha)(t-t_1)\right] + U_p\right] + O(\epsilon^2), \tag{5.1a}$$

$$F^s = \epsilon\left[-kA^s\exp\left[-k(t-t_1)\right] + F_p\right] + O(\epsilon^2), \tag{5.1b}$$

$$G^s = G_s + \epsilon\left[B\exp\left[-\epsilon(r+\alpha)(t-t_1)\right] + G_p\right] + O(\epsilon^2), \tag{5.1c}$$

where
$$U_p = -\frac{(U_s-1)^2 - \omega^2}{\omega(\omega^2+k^2)}\tau_1\sin\omega t, \tag{5.2a}$$

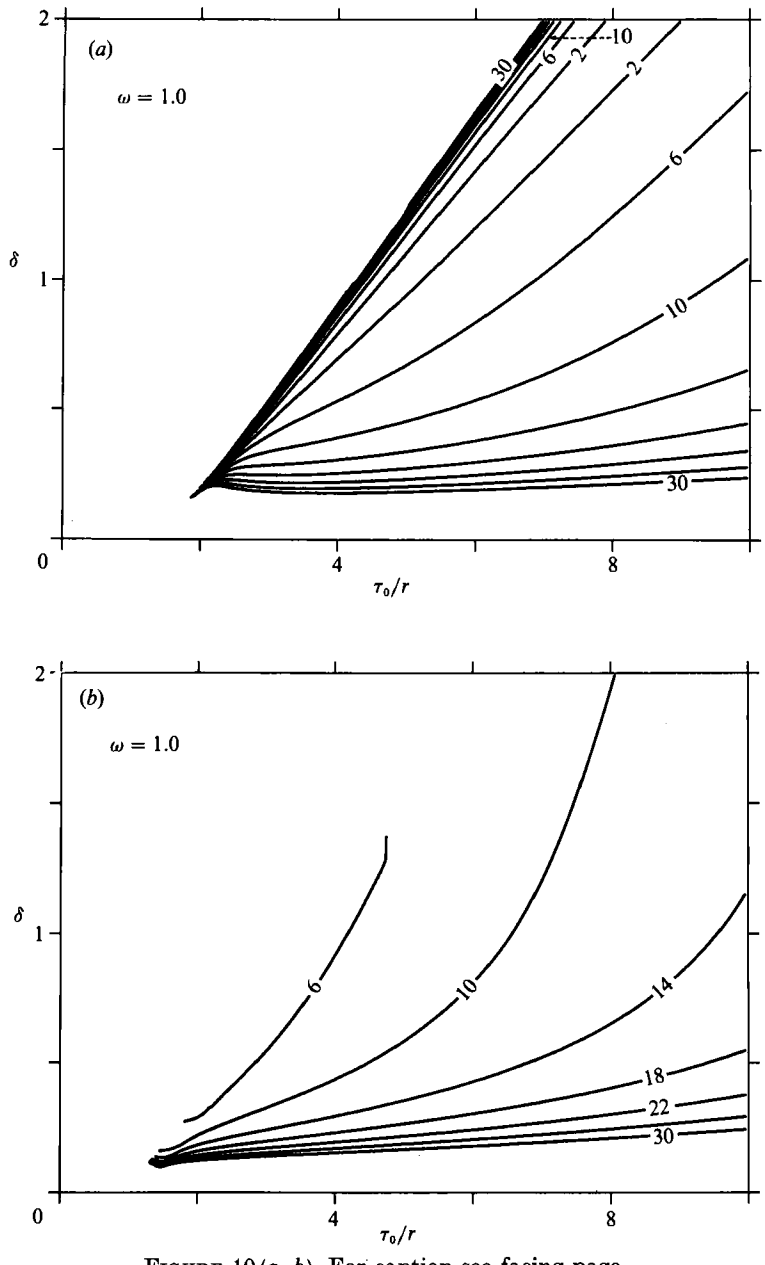

FIGURE 10 (*a*, *b*). For caption see facing page.

$$F_p = rU_s - \tau_0 - \frac{(U_s-1)^2+k^2}{\omega^2+k^2}\tau_1 \cos\omega t, \tag{5.2b}$$

$$G_p = \frac{(U_s-1)}{\omega}\tau_1 \sin\omega t, \tag{5.2c}$$

while those to solutions in $W_\epsilon^u(p)$ for $t\in(-\infty, t_2]$ are

$$U^u = U_s + \epsilon[A^u \exp[k(t-t_2)] + U_p] + O(\epsilon^2), \tag{5.3a}$$

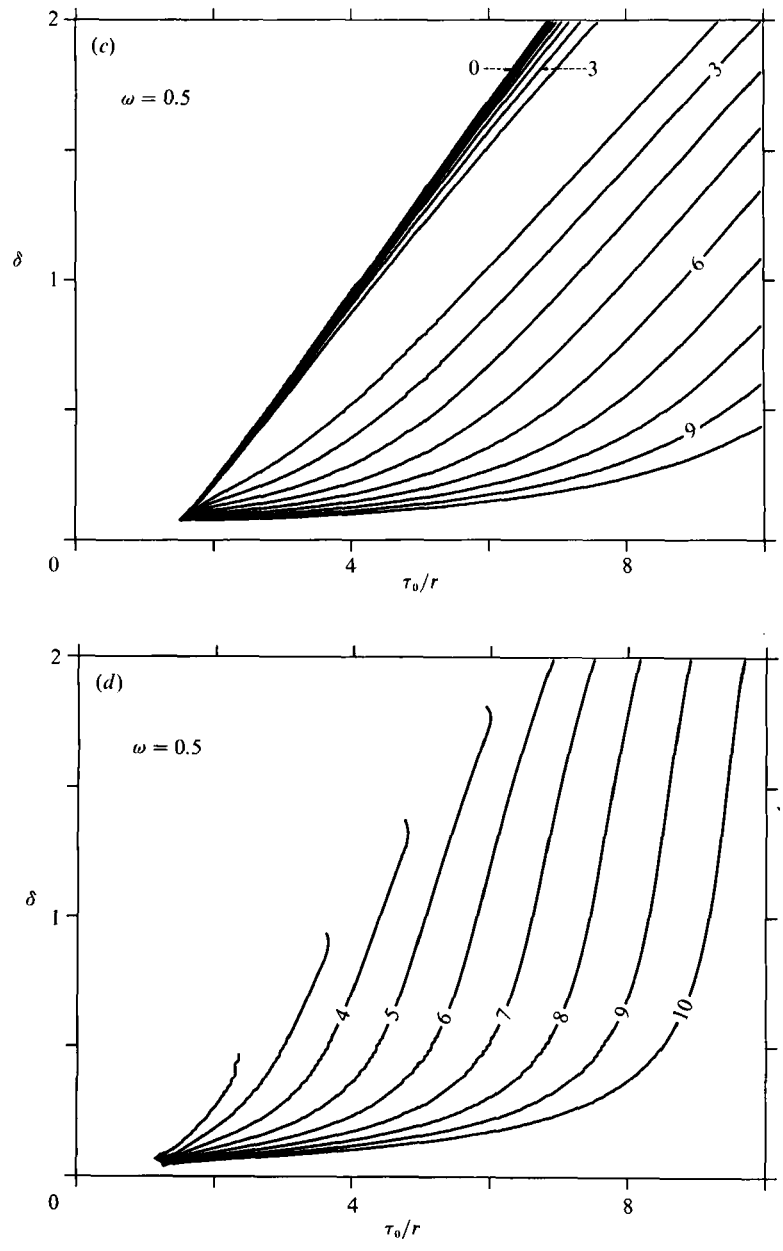

FIGURE 10. Contours of $(\tau_1/r)_c^{\pm}$ from (4.24) as a function of τ_0/r and δ for $\omega = 1.0$ and $\omega = 0.5$. The superscripts $\pm$ refer to perturbations about the right (+) or left (−) lobes of the separatrix. (*a*) $(\tau_1/r)_c^+$ for $\omega = 1.0$, (*b*) $(\tau_1/r)_c^-$ for $\omega = 1.0$, (*c*) $(\tau_1/r)_c^+$ for $\omega = 0.5$, (*d*) $(\tau_1/r)_c^-$ for $\omega = 0.5$.

$$F^{\mathrm{u}} = \epsilon[kA^{\mathrm{u}} \exp[k(t-t_2)] + F_p] + O(\epsilon^2), \tag{5.3b}$$

$$G^{\mathrm{u}} = G_{\mathrm{s}} + \epsilon G_p + O(\epsilon^2). \tag{5.3c}$$

Note that as $t \to \infty$ in (5.1) and $t \to -\infty$ in (5.3), the exponential terms vanish and the solutions converge to the order-ϵ periodic oscillation p, for which (4.3) and (3.3) yield the first-order approximation $(U^{\mathrm{s,u}}, F^{\mathrm{s,u}}, G^{\mathrm{s,u}}) = (U_{\mathrm{s}}, 0, G_{\mathrm{s}}) + O(\epsilon)$. The terms in (5.1) and (5.3) with coefficients A^{s} and A^{u} are the linear approximations (3.9) to the

separatrix wave, which is a homogeneous solution of the perturbation equations (B 4). The terms in (5.1) with coefficient B describe the slow evolution associated with the stability (in γ_ϵ) of p that was demonstrated in (4.4) and (4.5).

The variational equations for $\boldsymbol{q}_1^{\mathrm{s,u}}$, obtained by linearizing (2.9) about $\boldsymbol{q}_0$ and neglecting higher-order terms, are

$$\frac{\mathrm{d}V_1^{\mathrm{s,u}}}{\mathrm{d}t} = F_1^{\mathrm{s,u}} + g_1(\boldsymbol{q}_0, t), \tag{5.4a}$$

$$\frac{\mathrm{d}F_1^{\mathrm{s,u}}}{\mathrm{d}t} = [k^2 - 3(U_\mathrm{s}-1)\,V_0 - \tfrac{3}{2}V_0^2]\,V_1^{\mathrm{s,u}} + (U_\mathrm{s}-1+V_0)\,G_1^{\mathrm{s,u}} + g_2(\boldsymbol{q}_0, t), \tag{5.4b}$$

$$\frac{\mathrm{d}G_1^{\mathrm{s,u}}}{\mathrm{d}t} = g_3(\boldsymbol{q}_0, t), \tag{5.4c}$$

where $V_0 = V_{0\pm}(t-t_0)$ on the separatrix solution $\boldsymbol{q}_0$, and from (2.15),

$$g_1(\boldsymbol{q}_0, t) = -rV_0 - (rU_\mathrm{s} - \tau_0) + \tau_1 \cos\omega t, \tag{5.5a}$$

$$g_2(\boldsymbol{q}_0, t) = -rF_0, \tag{5.5b}$$

$$g_3(\boldsymbol{q}_0, t) = g_3' + (U_\mathrm{s}-1)\,\tau_1 \cos\omega t, \tag{5.5c}$$

$$g_3'(\boldsymbol{q}_0, t) = -(rU_\mathrm{s} - \tau_0)\,V_0 - \tfrac{1}{2}rV_0^2 + V_0\tau_1 \cos\omega t. \tag{5.5d}$$

It may be verified that (5.4) and (3.7) combine to give (4.19).

Because $\boldsymbol{q}_1^{\mathrm{s}}$ in general contains variations on an ϵt timescale as indicated by (5.1), however, a uniformly valid solution for $\boldsymbol{q}_1^{\mathrm{s}}$ over $t \in [t_0, \infty)$ cannot be obtained from (5.4) alone. This is readily seen as follows. The integration of (5.4c) gives

$$G_1^{\mathrm{s}}(t, t_0) = C_0^{\mathrm{s}} - \int_t^\infty g_3'\,\mathrm{d}t' + G_p, \quad t \in [t_0, \infty), \tag{5.6a}$$

$$G_1^{\mathrm{u}}(t, t_0) = C_0^{\mathrm{u}} + \int_{-\infty}^t g_3'\,\mathrm{d}t' + G_p, \quad t \in (-\infty, t_0], \tag{5.6b}$$

where $C_0^{\mathrm{s,u}}$ are constants and G_p is defined in (5.2c). If we apply (4.11b) to (5.6a, b), we obtain

$$C_0^{\mathrm{s}} - C_0^{\mathrm{u}} = \int_{-\infty}^\infty g_3'\,\mathrm{d}t, \tag{5.7}$$

which will be non-zero in general. For non-zero values of either C_0^{s} or C_0^{u} it is clear from the form of (5.6a, b) and of (5.1) and (5.3) that the corresponding solutions (5.6a, b) are not valid within $O(\epsilon)$ of p. This is also indicated by the fact that (5.6a, b) with $C_0^{\mathrm{s,u}} \neq 0$ are not uniformly valid approximate solutions of (2.9c) for $|\epsilon(t-t_0)| > O(1)$.

Regular perturbation procedures evidently are not sufficient to give a complete determination of G_1^{s} and singular perturbation methods must be utilized so that (4.7a, b) represent general asymptotic expansions (Kevorkian & Cole 1981). The equations (5.4c) only give a valid approximation for G_1^{s} for $\epsilon(t-t_0) < O(1)$. For $\epsilon(t-t_0) \geqslant O(1)$, the $O(\epsilon^2)$ linear terms in G_1^{s} and V_1^{s} from (2.9c) that give rise in (5.1) to variations on the ϵt timescale need to be considered for the full determination of G_1^{s}. Consequently, in order for (5.4) to contain a complete description of the perturbation $\boldsymbol{q}_1^{\mathrm{s}}$, (5.4$c$) must be modified to include $O(\epsilon^2)$ linear terms that are important within $O(\epsilon)$ of p,

$$\frac{\mathrm{d}G_1^{\mathrm{s,u}}}{\mathrm{d}t} = g_3^{\mathrm{s,u}}(\boldsymbol{q}_0, \boldsymbol{q}_1^{\mathrm{s}}, t), \tag{5.8a}$$

where

$$g_3^{\mathrm{u}}(\boldsymbol{q}_0, t) = g_3(\boldsymbol{q}_0, t), \tag{5.8b}$$

$$g_3^{\mathrm{s}}(\boldsymbol{q}_0, \boldsymbol{q}_1^{\mathrm{s}}, t) = g_3(\boldsymbol{q}_0, t) + \epsilon h_3^{\mathrm{s}}(\boldsymbol{q}_1^{\mathrm{s}}), \tag{5.8c}$$

$$h_3^{\mathrm{s}}(\boldsymbol{q}_1) = -rG_1^{\mathrm{s}} - (rU_{\mathrm{s}} - \tau_0)\, V_1^{\mathrm{s}}. \tag{5.8d}$$

With (5.8*c*, *d*) the perturbations $\boldsymbol{q}_1^{\mathrm{s,u}}$ may be obtained from the solution of (5.4*a*, *b*) and (5.8). The formulation (5.4*a*, *b*) and (5.8) is useful primarily because it then may be seen directly from (4.16)—(4.19) that the additional terms $\epsilon h_3^{\mathrm{s}}$ in (5.8*c*), which were not considered by Wiggins & Holmes (1987) but which are necessary for a complete determination of G_1^{s}, will only contribute $O(\epsilon)$ terms to the Melnikov function and will not change any of the previous results. This is also consistent with the fact that (4.19) is given by the combination of (5.4) and (3.7).

Although the determination of $G_1^{\mathrm{s,u}}$ involves a singular perturbation problem, that problem is particularly straightforward in this case so that the nature of the solutions for $G_1^{\mathrm{s,u}}$ may be readily found from (5.1), (5.3), and (5.6). It is apparent from (5.1*c*) and (5.6*a*) that C_0^{s} is an approximate representation, for $\epsilon(t-t_0) < O(1)$ of $B\exp[-\epsilon(r+\alpha)(t-t_1)]$ and from (5.3*c*) and (5.6*b*) that $C_0^{\mathrm{u}} = 0$. Furthermore, the results in (5.1) and (5.3) may be simply combined with those from (5.6) to form the following uniformly valid approximate solutions, with $O(\epsilon)$ error, to (5.4*a*, *b*) and (5.8):

$$G_1^{\mathrm{s}}(t, t_0) = \tilde{C}_0^{\mathrm{s}} \exp[-\epsilon(r+\alpha)(t-t_0)] - \int_t^{\infty} g_3' \,\mathrm{d}t' + G_p, \quad t \in [t_0, \infty), \tag{5.9a}$$

$$G_1^{\mathrm{u}}(t, t_0) = \int_{-\infty}^{t} g_3' \,\mathrm{d}t' + G_p, \quad t \in (-\infty, t_0]. \tag{5.9b}$$

The consistency of (5.9*a*, *b*) is demonstrated in Appendix A.

It is possible, in addition, to determine the required value for $\tilde{C}_0^{\mathrm{s}}$ in (5.9*a*) for satisfaction of (4.10). Subtracting (5.9*a*, *b*) and using (4.11*b*), we obtain

$$\tilde{C}_0^{\mathrm{s}} = \int_{-\infty}^{\infty} g_3' \,\mathrm{d}t. \tag{5.10}$$

The substitution of (5.5*d*) in (5.10) gives

$$\tilde{C}_0^{\mathrm{s}} = -(rU_{\mathrm{s}} - \tau_0) \int_{-\infty}^{\infty} V_0 \,\mathrm{d}t - \tfrac{1}{2}r \int_{-\infty}^{\infty} V_0^2 \,\mathrm{d}t + \tau_1 \int_{-\infty}^{\infty} V_0 \cos\omega t \,\mathrm{d}t. \tag{5.11}$$

The integrals in (5.11) may be evaluated using (3.6) and the results combined with

$$C_1 = -(\tau_1/r)\, C_2 \cos\omega t_0, \tag{5.12}$$

which follows from setting $\Delta H_1(t_0) = 0$ in (4.23*a*), to eliminate $\cos\omega t_0$ and obtain

$$\tilde{C}_0^{\mathrm{s}} = r\left\{-(1-U_{\mathrm{s}})\, 8\tan^{-1}\left(\frac{V_{\mathrm{m}\pm}}{2k}\right) + \frac{4k\delta^2}{d}\right\}. \tag{5.13}$$

We will use (5.13) in the numerical solutions in §6 (see also Appendix C).

6. Numerical solutions

The analytical prediction (4.24) for the intersection of the manifolds is compared with results from numerical solutions in this section. The numerical solutions in the manifolds are obtained by integration of (2.9) forward in time from initial conditions

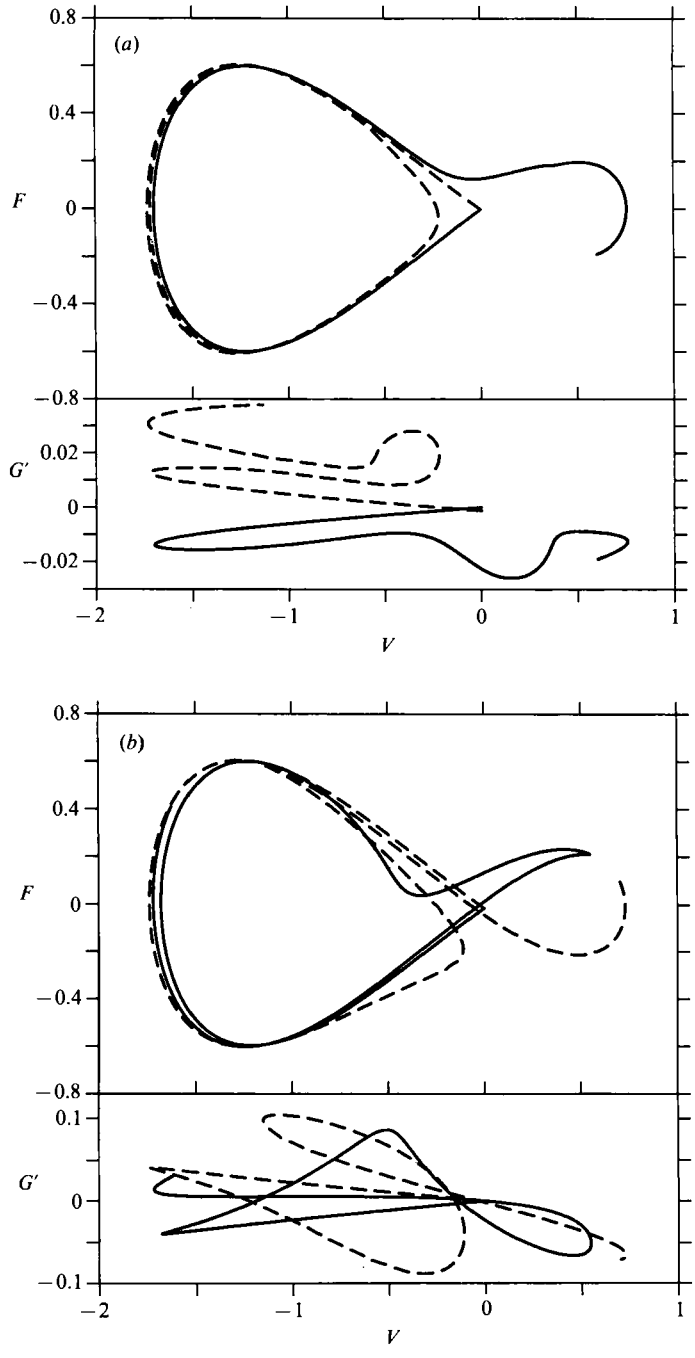

FIGURE 11. Phase-space projections on the (V,F)- and (V,G')-planes of a Poincaré section at time interval $2\pi/\omega$ of solutions in the stable $W^{s}_{\epsilon}(p)$ (dashed line) and unstable $W^{u}_{\epsilon}(p)$ (solid line) manifolds of p. The solutions are calculated numerically as explained in Appendix C. For clarity, only those solutions corresponding to the left lobe $(-)$ of the separatrix are shown. The parameters are $\delta = 0.3003$ and $\tau_0/r = 3.236$ so that $G_s = 0$ and $U_s = 1.236$. Also, $\omega = 1$ and $\epsilon = 0.005$. (*a*) $\tau_1 = 1$; $r = 0.2$ so that $\tau_1/r < (\tau_1/r)^{-}_{c} = 11.62$ and the manifolds do not intersect. (*b*) $\tau_1 = 10$, $r = 0.01$ so that $\tau_1/r > (\tau_1/r)^{-}_{c}$ and the manifolds intersect. The initial values of $G'^{s,u}$ do not coincide exactly at the homoclinic point near $G' = 0$ because much of the variation of G'^{s} on the ϵt timescale is not included in the numerical calculations, but is represented by the approximate initial conditions (Appendix C).

on the linear approximation (5.3) to the unstable manifold and backward in time from initial conditions on the linear approximation (5.1) to the stable manifold. This allows the description of the perturbed manifolds to be extended to the nonlinear regime. More details of the numerical solution procedures are given in Appendix C. The estimate (5.13) of the value of $\tilde{C}_0^{\rm s}$ in (5.9*a*) allows us to start the calculation of the stable manifold solutions in the particular direction, represented by the choice of $A^{\rm s}/B$ in (5.1), that gives the solutions in the stable manifold that intersect the unstable manifold if (4.24) is satisfied.

For the numerical calculations we specify $\delta = 0.3003$ and choose $\tau_0/r = 3.236$ so that $G_{\rm s} = 0$ and (3.3) is easily solved to give $U_{\rm s} = \frac{1}{2}[3-(1-8\delta^2)^{\frac{1}{2}}] = 1.236$. This value of δ and $G = 0$ were used in figure 2 and for the contour plot of $\hat{H}(U, F; G)$ in figure 3(*b*). In figure 4, this value of δ was used for the plot of the steady frictional response (3.13) with $\epsilon r = 10^{-4}$. A line at $\tau_0/r = 3.236$ is also shown in figure 4 indicating the U-values of the three steady solutions in this case. In the numerical solutions, we also take $\omega = 1$ and vary the parameters τ_1, r and ϵ. The variables

$$(V, F, G') = (U-U_{\rm s}, F, G-G_{\rm s}), \tag{6.1}$$

are utilized so that the unstable periodic oscillation is near the origin $(0, 0, 0)$.

Figure 11 shows phase-space projections on the (V, F)- and (V, G')-planes of a Poincaré section of the solutions in the stable and unstable manifolds for $\epsilon = 0.005$ and for two different sets of parameter values corresponding to $\tau_1/r < (\tau_1/r)_{\rm c}^-$ and to $\tau_1/r > (\tau_1/r)_{\rm c}^-$. For clarity, only the stable and unstable manifolds corresponding to the left lobe $(-)$ of the separatrix are shown, since $(\tau_1/r)_{\rm c}^- < (\tau_1/r)_{\rm c}^+$ for this value of τ_0/r and δ (figure 10). For an intersection of $W_\epsilon^{\rm s}(p)$ and $W_\epsilon^{\rm u}(p)$ to occur, the solutions have to coincide in all three variables (V, F, G') of the Poincaré section. For $(\tau_1/r) < (\tau_1/r)_{\rm c}^-$, the solutions plotted do not intersect, while for $(\tau_1/r) > (\tau_1/r)_{\rm c}^-$, they do (within the accuracy of the approximations involved in choosing $\tilde{C}_0^{\rm s}$), but the agreement of the (V, F) and (V, G') intersections is a little difficult to see in this plot. We take a closer look at the intersections below. Note that the initial values for $G'^{\rm s,\,u}$ do not coincide exactly at the homoclinic point. This is because much of the variation on the et timescale in (5.1*c*) is not included in the numerical calculation, but is represented by the approximate initial conditions (Appendix C). In figure 12, we examine the intersections and determine the dependence of these on the values of τ_1/r. We specify $\epsilon = 0.001$ and restrict the plots to (F, V) and (F, G') phase-space projections near the origin. Again only the solutions corresponding to the left lobe of the separatrix are shown. For these values of the parameters, (4.24) predicts intersection for $r < 0.086$, which is observed. Note that to the accuracy of the plots, the intersections occur at the same values of F in both the (V, F) and in the (G', F) projections, reflecting the intersection of the manifolds in the three-dimensional Poincaré section.

Time series of V calculated from (2.9) with initial conditions of $V = F = G' = 0$ at $t = 0$ for $\epsilon = 0.01$ and for different values of τ_1 and r are shown in figure 13. These include one case with $\tau_1/r < (\tau_1/r)_{\rm c}^{\pm}$ and three with $\tau_1/r > (\tau_1/r)_{\rm c}^{\pm}$. The time series are either regular or (transiently) chaotic as predicted. The three cases with different values of $\tau_1/r > (\tau_1/r)_{\rm c}^{\pm}$ are shown to illustrate the increase in the strength of the irregular behaviour for increasing τ_1/r. The calculations for V with $\tau_1 = 10$, $r = 0.01$ in the bottom plot in figure 13 are extended to longer time in figure 14. The chaotic behaviour is evident to about $t \approx 3300$, when the solution begins a regular approach to a stable periodic oscillation near the location of the large-amplitude steady

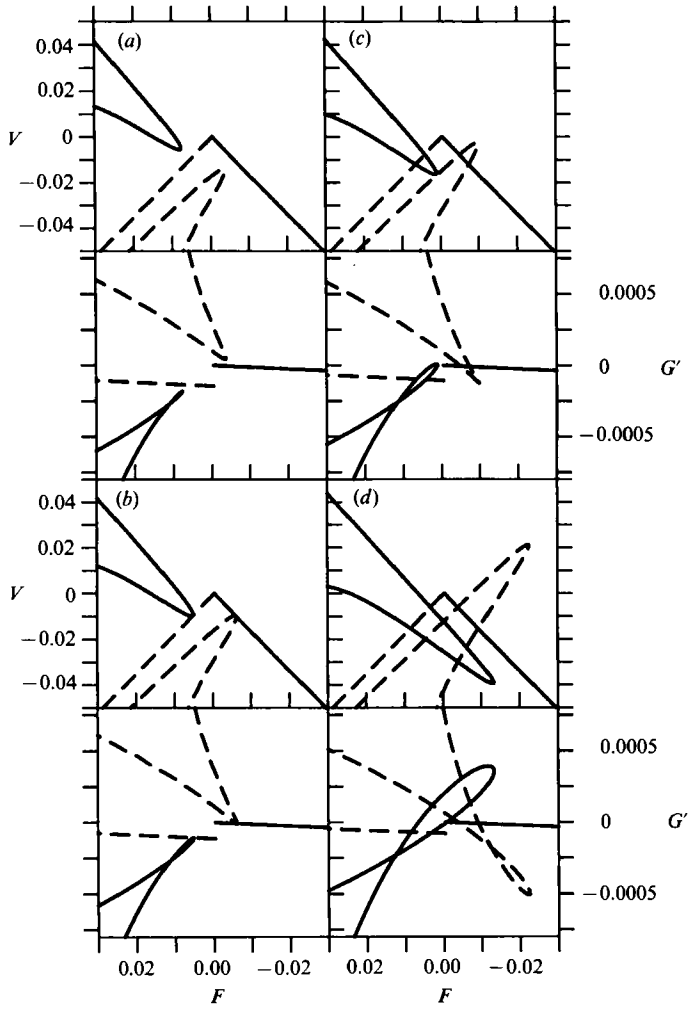

FIGURE 12. Phase-space projections on (F, V)- and (F, G')-planes of a Poincaré section at time intervals $2\pi/\omega$ of solutions in the stable $W^{s}_{\epsilon}(p)$ (dashed line) and unstable $W^{u}_{\epsilon}(p)$ (solid line) manifolds of p similar to figure 11. The values of δ, τ_0/r, and ω are the same as figure 11. Here, $\epsilon = 0.001$ and $\tau_1 = 1$. Only the region near the origin and the $(-)$ solutions are shown to clearly illustrate the variation in behaviour with τ_1/r and to show intersections in all three variables (V, F, G'). As in figure 11, the initial values of $G'^{s,u}$ do not coincide at the homoclinic point near $G' = 0$ because much of the variation of G'^{s} on the ϵt timescale is not included in the numerical calculations, but is represented by the approximate initial conditions (Appendix C). (*a*) $r = 0.09$, (*b*) $r = 0.086$, (*c*) $r = 0.08$, (*d*) $r = 0.06$. For these cases, $(\tau_1/r)^{-}_{c} = 11.63$ so that intersection is predicted for $r < 0.086$, which is found. Note that within the accuracy of the approximate initial conditions (Appendix C) the intersections occur at the same value of F in the (F, V)- and (F, G')-planes reflecting the intersection of the stable and unstable manifolds in the three-dimensional Poincaré section.

frictional response. It is important to note that eventually nearly all solutions will asymptote to regular behaviour even when chaotic solutions exist in the model according to (4.24). This occurs because the chaotic invariant set is not attracting, but of saddle-type stability. The existence of strange attractors in the model is not implied by the satisfaction of the Melnikov criterion. The time series of V in figure

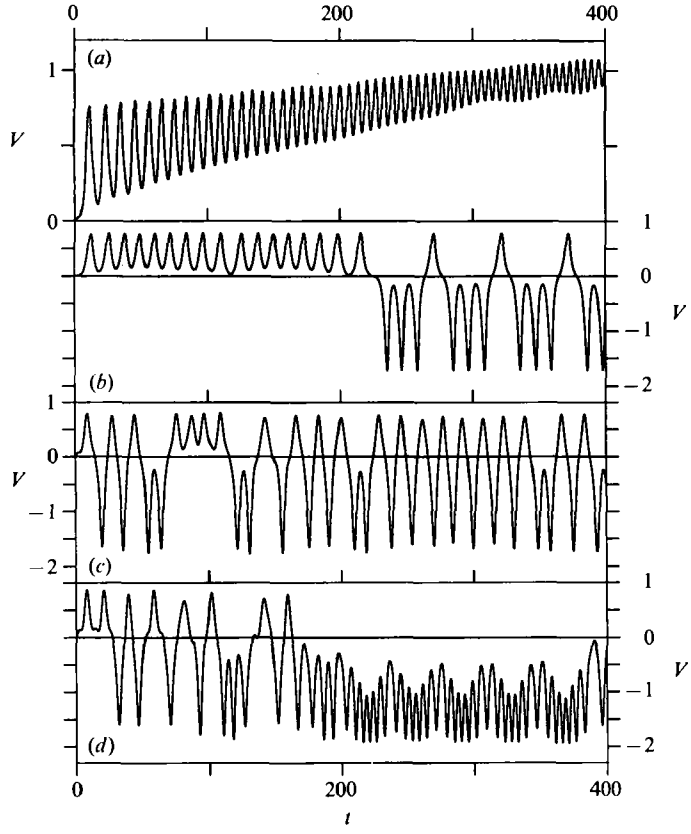

FIGURE 13. Time-series solutions for V calculated from (2.9) with initial conditions $V = F = G' = 0$ at $t = 0$. Values of δ, τ_0/r and ω are the same as in figure 11. Here, $\epsilon = 0.01$ and τ_1 and r are varied. For (*a*) $(\tau_1/r) < (\tau_1/r)_c^{\pm}$ and the solution involves a regular approach to a stable periodic oscillation near the location of the large amplitude steady frictional response. For (*b–d*) $(\tau_1/r) > (\tau_1/r)_c^{\pm}$ and the solutions are chaotic. (*a*) $\tau_1 = 1, r = 0.1$, (*b*) $\tau_1 = 1, r = 0.01$, (*c*) $\tau_1 = 5, r = 0.01$, (*d*) $\tau_1 = 10, r = 0.01$.

14 illustrates this point, but also shows that the irregular behaviour can be quite long-lived.

To show variations in chaotic behaviour with ϵ for fixed τ_1/r, we plot time-series calculations of V with $\tau_1 = 10$, $r = 0.01$ for $\epsilon = 0.001$ and $\epsilon = 0.1$ in figures 15 and 16 for comparison with V in figure 14, where $\epsilon = 0.01$. The behaviour is more erratic with the larger ϵ. The initial values for the calculation with $\epsilon = 0.001$ in figure 15 were $V = -0.2$, $F = -1.95 \times 10^{-3}$, $G' = 0$, and the time series for V remained chaotic to at least $t = 5000$. The initial values for the calculation in figure 16 with $\epsilon = 0.1$ were $(V, F, G') = (0, 0, 0)$ and the time series for V clearly shows chaotic behaviour. A Poincaré section of the solution in figure 15 projected on the (V, F)- and (V, G')-planes is shown in figure 17. The extent to which F and V stay close to the unperturbed separatrix and the fact that G' remains small in this small-ϵ case are clearly evident. Extreme sensitivity of the solutions to the initial conditions was found in making these calculations. Very small changes in initial values near the unstable periodic orbit $(V, F, G') = (0, 0, 0)$ led to totally different long-time behaviour. To check that the above solutions were accurately characterized as chaotic or regular, exponential

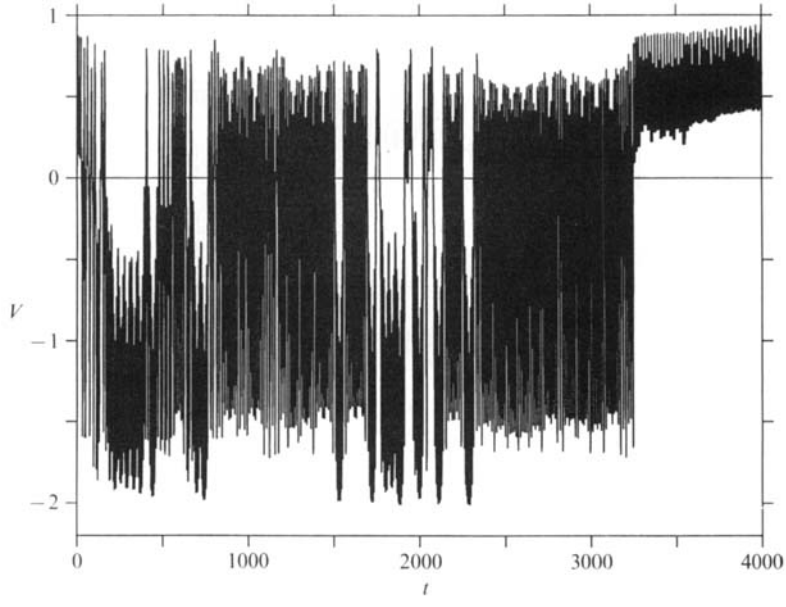

FIGURE 14. An extension to longer time of the time series shown in figure 13(*d*), i.e. with $\omega = 1$, $\epsilon = 0.01$, $\tau_1 = 10$ and $r = 0.01$. This solution is chaotic to $t \approx 3300$ when it starts a regular approach to the stable periodic oscillation near the large amplitude steady frictional response.

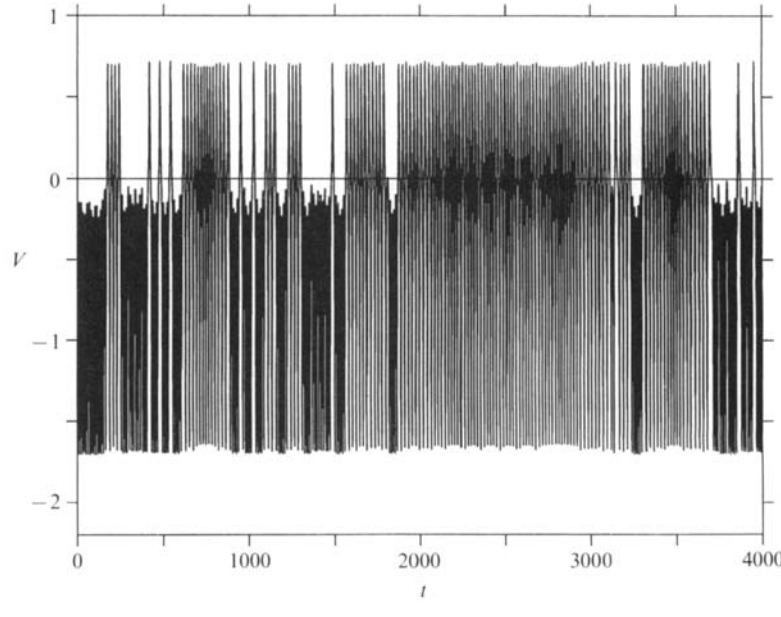

FIGURE 15. Time-series solution for V at the same value of δ, τ_0/r, ω, τ_1 and r as in figure 14 but with $\epsilon = 0.001$ here (see also figure 17).

growth rates of perturbations ('local Lyapunov exponents') were calculated continuously as a function of time using the method of Wolf *et al.* (1985). Persistently positive values of one exponent were found for the solutions termed chaotic in agreement with the predictions of (4.24) and the visual evidence for irregularity of the time series.

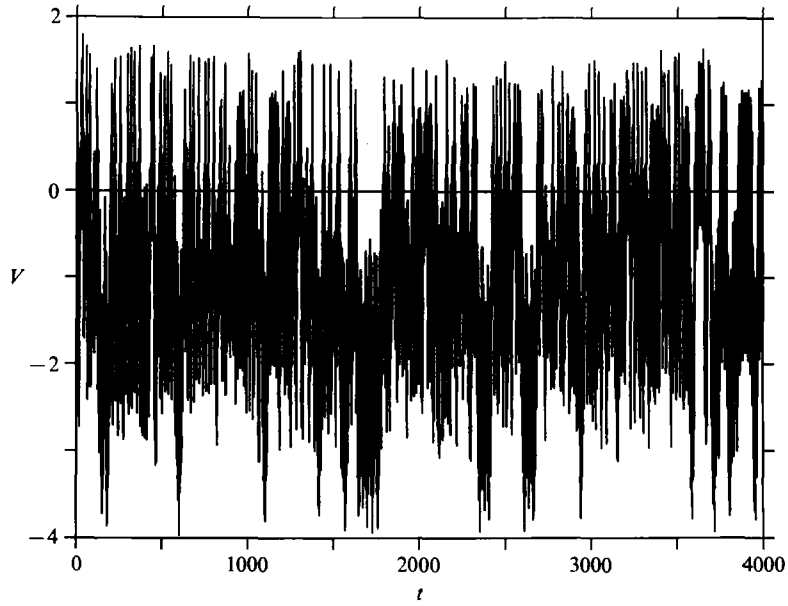

FIGURE 16. Time series of V at the same values of δ, τ_0/r, ω, τ_1 and r as in figures 14 and 15, but with $\epsilon = 0.1$ here.

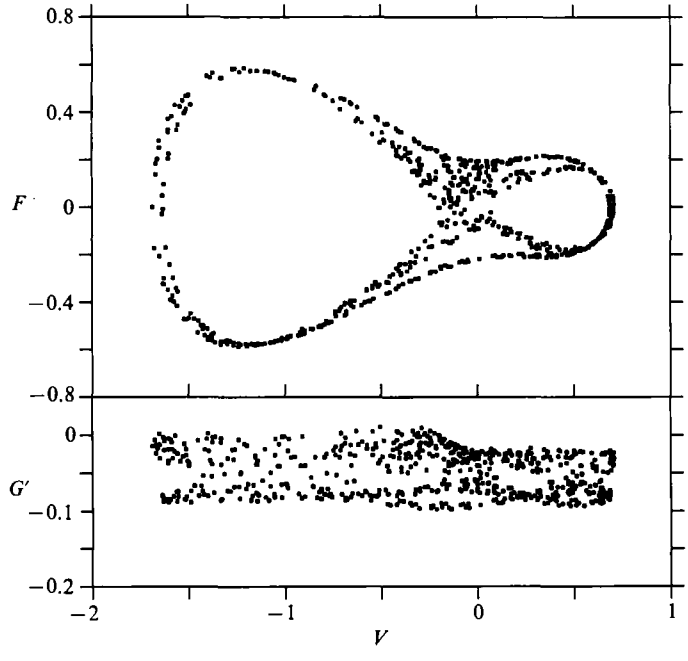

FIGURE 17. Phase-space projections on the (V, F)- and (V, G')-planes of the Poincaré section at time interval $2\pi/\omega$ for the solution shown as a time series of V in figure 15 with $\epsilon = 0.001$ for $0 \leqslant t \leqslant 4000$.

7. Summary

The existence of chaotic solutions in a systematically derived model of forced quasi-geostrophic flow over anisotropic topography has been demonstrated analytically and verified numerically. The chaos is characterized by flow that switches

randomly between three oscillatory nonlinear free-wave regimes. The result is of interest because it proves that the response of a simple model of coastal ocean currents to regular forcing can be irregular.

Note that although the chaotic solutions found here are not attractors, the region of parameter space for which (4.24) predicts that they occur is extensive. This differs from the situation studied by Samelson & Allen (1987) where, for the same model with $\tau_0 = 0$ and ω near resonance, a strange attractor was found to exist in a very limited region of parameter space. On the other hand, in the present case when chaotic behaviour is possible by (4.24), the nature (chaotic or regular) of the solutions depends critically on the exact choice of initial values. A chaotic attractor could arise through a change in (global) stability of one of the chaotic solutions found here, but we do not pursue this possibility here.

Whether there is a connection between the observed lack of regularity of coastal ocean currents and the chaotic behaviour found in idealized dynamical models such as the one considered here, remains unclear. We suggest that the study of a sequence of increasingly complex theoretical or laboratory models of forced quasi-geostrophic flow over topography might provide a fruitful approach for addressing that question.

This research was supported for J.S.A. and P.A.N. by the National Science Foundation (NSF) under Grant OCE-8620403 and by the Office of Naval Research (ONR) Coastal Sciences Program under Contract N00014-90-J-1050, and for R.M.S. by ONR under Contract N00014-84-C-0134 NR083-400 and by NSF under Grant OCE-8916463. The authors are grateful to S. Wiggins and R. Guenther for helpful discussions. They also thank M. Lucas, F. Beyer and M. Stewart for typing the manuscript. Woods Hole Oceanographic Institution Contribution No. 7343.

Appendix A. Perturbation solutions in $W^{s}_{\epsilon}(p)$ and $W^{u}_{\epsilon}(p)$

Solutions for the $O(\epsilon)$ perturbation variables (4.9) $\boldsymbol{q}_1^{s,u} = (V_1^{s,u}, F_1^{s,u}, G_1^{s,u})$ that satisfy (5.4a, b) and (5.8) with $O(\epsilon)$ error are found here. Based on the arguments in §5, we assume that G_1^{s} and G_1^{u} are given by (5.9a, b) and we solve (5.4a, b) for $V_1^{s,u}$ and $F_1^{s,u}$. The consistency of the representations (5.9a, b) for $G_1^{s,u}$ will be checked by verifying that additional corrections to $\boldsymbol{q}_\epsilon^{s,u}$ implied by the resultant solutions for $\epsilon\boldsymbol{q}_1^{s,u}$ are $O(\epsilon^2)$ and that the limits of $\boldsymbol{q}_0 + \epsilon\boldsymbol{q}_1^{s}$ for $t \to \infty$ and $\boldsymbol{q}_0 + \epsilon\boldsymbol{q}_1^{u}$ for $t \to -\infty$ agree with (5.1) and (5.3) respectively. The perturbation solutions $\boldsymbol{q}_1^{s,u}$ so obtained thus represent the $O(\epsilon)$ terms in a general asymptotic expansion (Kevorkian & Cole 1981) for $\boldsymbol{q}_\epsilon^{s,u}$. We also illustrate how the Melnikov integral (4.21) may be obtained by satisfying (4.10) directly. This latter procedure has some similarities to that used in the analysis of Chow, Hale & Mallet-Paret (1980) in a two-variable case.

We first consider solutions in W^{u}_{ϵ} for $t \in (-\infty, t_0]$. We assume G_1^{u} is given by (5.9b) and let

$$V_1^{u} = \hat{V}_1^{u} + U_p, \quad F_1^{u} = \hat{F}_1^{u} + F_p, \tag{A 1a, b}$$

so that (5.4a, b) become

$$\frac{\mathrm{d}\hat{V}_1^{u}}{\mathrm{d}t} = \hat{F}_1^{u} + g_1', \quad \frac{d\hat{F}_1^{u}}{\mathrm{d}t} = [k^2 - 3(U_s - 1)\,V_0 - \tfrac{3}{2}V_0^2]\,\hat{V}_1^{u} + g_2^{u}, \tag{A 2a, b}$$

where

$$g_1' = -rV_0, \tag{A 3a}$$

$$g_2^{u} = -rF_0 - [3(U_s - 1)\,V_0 + \tfrac{3}{2}V_0^2]\,U_p + (U_s - 1 + V_0)\int_{-\infty}^{t} g_3'\,\mathrm{d}t' + V_0\,G_p. \tag{A 3b}$$

A first integral of (A 2) may be found, in a manner similar to (4.19) and (4.20), by combining (A 2) and (3.7) to give,

$$\frac{\mathrm{d}}{\mathrm{d}t}\left[\hat{V}_1^{\mathrm{u}}\frac{\partial H}{\partial U}+\hat{F}_1^{\mathrm{u}}\frac{\partial H}{\partial F}\right]=g_1'\frac{\partial H}{\partial U}+g_2^{\mathrm{u}}\frac{\partial H}{\partial F}, \tag{A 4}$$

where H is defined in (4.13) and all derivatives of H are evaluated at $\boldsymbol{q}_0$ as in (4.18). Integration of (A 4) from $-\infty$ to t and use of (4.14b) gives

$$\hat{V}_1^{\mathrm{u}}\frac{\partial H}{\partial U}+\hat{F}_1^{\mathrm{u}}\frac{\partial H}{\partial F}=\int_{-\infty}^{t}\left(g_1'\frac{\partial H}{\partial U}+g_2^{\mathrm{u}}\frac{\partial H}{\partial F}\right)\mathrm{d}t'. \tag{A 5}$$

With (A 2a) and (3.7a, b), (A 5) may be written

$$F_0\frac{\mathrm{d}V_1^{\mathrm{u}}}{\mathrm{d}t}-\frac{\mathrm{d}F_0}{\mathrm{d}t}\hat{V}_1^{\mathrm{u}}=F_0^2\frac{\mathrm{d}}{\mathrm{d}t}\left(\frac{\hat{V}_1^{\mathrm{u}}}{F_0}\right)=g_1'F_0+\int_{-\infty}^{t}\left(g_1'\frac{\partial H}{\partial U}+g_2^{\mathrm{u}}\frac{\partial H}{\partial F}\right)\mathrm{d}t'. \tag{A 6}$$

The apparent difficulty around the singular point is circumvented by introducing a cutoff function and passing to the limit in the standard way.

The solution of (A 6) for $\hat{V}_1^{\mathrm{u}}$ is

$$\hat{V}_1^{\mathrm{u}}=C_1^{\mathrm{u}}F_0+F_0\int\frac{1}{F_0^2}\left[\int_{-\infty}^{t'}F_0\left(\frac{\mathrm{d}g_1'}{\mathrm{d}t''}+g_2^{\mathrm{u}}\right)\mathrm{d}t''\right]\mathrm{d}t', \tag{A 7}$$

where C_1^{u} is a constant, the last term has been left as an indefinite integral, and integration by parts together with (3.7b) have been used on the $g_1'\partial H/\partial U$ term in (A 6). The equation (A 7) may be written in a more convenient form if we define a function L_0 such that

$$\frac{\mathrm{d}L_0}{\mathrm{d}t}=\frac{1}{F_0^2}, \tag{A 8}$$

and use integration by parts. The result is

$$\hat{V}_1^{\mathrm{u}}(t,t_0)=C_1^{\mathrm{u}}F_0+F_0L_0\int_{-\infty}^{t}F_0\left(\frac{\mathrm{d}g_1'}{\mathrm{d}t'}+g_2^{\mathrm{u}}\right)\mathrm{d}t'+F_0\int_{t}^{t_0}F_0L_0\left(\frac{\mathrm{d}g_1'}{\mathrm{d}t'}+g_2^{\mathrm{u}}\right)\mathrm{d}t', \tag{A 9a}$$

where limits have now been placed on all integrals. An explicit expression for L_0 is given at the end of this Appendix. The corresponding solution for $\hat{F}_1^{\mathrm{u}}$ may be found from (A 9a) and (A 2a):

$$\hat{F}_1^{\mathrm{u}}(t,t_0)=C_1^{\mathrm{u}}\frac{\mathrm{d}F_0}{\mathrm{d}t}-g_1'+\frac{\mathrm{d}}{\mathrm{d}t}(F_0L_0)\int_{-\infty}^{t}F_0\left(\frac{\mathrm{d}g_1'}{\mathrm{d}t'}+g_2^{\mathrm{u}}\right)\mathrm{d}t'+\frac{\mathrm{d}F_0}{\mathrm{d}t}\int_{t}^{t_0}F_0L_0\left(\frac{\mathrm{d}g_1'}{\mathrm{d}t'}+g_2^{\mathrm{u}}\right)\mathrm{d}t'. \tag{A 9b}$$

Note that the homogeneous solution for $\boldsymbol{q}_1^{\mathrm{u}}$ is $C_1^{\mathrm{u}}\mathrm{d}\boldsymbol{q}_0/\mathrm{d}t$.

The limiting behaviour for $V_1^{\mathrm{u}}(t\to-\infty)$ may be obtained by substituting the asymptotic expressions (3.11) for F_0 and V_0 in (A 7) and evaluating the integrals. Agreement with (5.3a) is found. Similar agreement with (5.3b) is found for $F_1^{\mathrm{u}}(t\to-\infty)$.

For the solutions in W_ϵ^{s} for $t\in[t_0,\infty)$, we assume G_1^{s} is given by (5.9a) and write

$$V_1^{\mathrm{s}}=\hat{V}_1^{\mathrm{s}}-\tilde{C}_0^{\mathrm{s}}(U_{\mathrm{s}}-1)\,k^{-2}\exp\left[-\epsilon(r+\alpha)(t-t_0)\right]+U_p,\quad F_1^{\mathrm{s}}=\hat{F}_1^{\mathrm{s}}+F_p, \tag{A 10a, b}$$

so that (5.4a, b) become

$$\frac{\mathrm{d}\hat{V}_1^{\mathrm{s}}}{\mathrm{d}t} = \hat{F}_1^{\mathrm{s}} + g_1', \quad \frac{\mathrm{d}\hat{F}_1^{\mathrm{s}}}{\mathrm{d}t} = [k^2 - 3(U_{\mathrm{s}}-1)\,V_0 - \tfrac{3}{2}V_0^2]\,\hat{V}_1^{\mathrm{s}} + g_2^{\mathrm{s}}, \qquad \text{(A 11}a, b\text{)}$$

where

$$g_2^{\mathrm{s}} = -rF_0 - [3(U_{\mathrm{s}}-1)\,V_0 + \tfrac{3}{2}V_0^2]\,U_p - (U_{\mathrm{s}}-1+V_0)\int_t^\infty g_3'\,\mathrm{d}t' + V_0 G_p$$
$$+ \tilde{C}_0^{\mathrm{s}} \exp[-\epsilon(r+\alpha)(t-t_0)]\,V_0\{(U_{\mathrm{s}}-1)\,k^{-2}[3(U_{\mathrm{s}}-1)+\tfrac{3}{2}V_0]+1\}. \quad \text{(A 12)}$$

Following a procedure similar to that used to obtain (A 9a, b), we find

$$\hat{V}_1^{\mathrm{s}}(t,t_0) = C_1^{\mathrm{s}} F_0 - F_0 L_0 \int_t^\infty F_0\left(\frac{\mathrm{d}g_1'}{\mathrm{d}t'} + g_2^{\mathrm{s}}\right)\mathrm{d}t' - F_0 \int_{t_0}^t F_0 L_0\left(\frac{\mathrm{d}g_1'}{\mathrm{d}t'} + g_2^{\mathrm{s}}\right)\mathrm{d}t', \quad \text{(A 13}a\text{)}$$

$$\hat{F}_1^{\mathrm{s}}(t,t_0) = C_1^{\mathrm{s}}\frac{\mathrm{d}F_0}{\mathrm{d}t} - g_1' - \frac{\mathrm{d}}{\mathrm{d}t}(F_0 L_0)\int_t^\infty F_0\left(\frac{\mathrm{d}g_1'}{\mathrm{d}t'} + g_2^{\mathrm{s}}\right)\mathrm{d}t' - \frac{\mathrm{d}F_0}{\mathrm{d}t}\int_{t_0}^t F_0 L_0\left(\frac{\mathrm{d}g_1'}{\mathrm{d}t'} + g_2^{\mathrm{s}}\right)\mathrm{d}t'. \quad \text{(A 13}b\text{)}$$

The limiting behaviour for $V_1^{\mathrm{s}}(t\to\infty)$ and $F_1^{\mathrm{s}}(t\to\infty)$ is in agreement with (5.1a, b).

It is conceptually useful to see how the condition (4.22) for the intersection of $W_\epsilon^{\mathrm{s}}(p)$ and $W_\epsilon^{\mathrm{u}}(p)$, i.e. for (4.10) to be satisfied, is obtained from (A 9), (A 13) and (5.9a, b). The constants $C_1^{\mathrm{s,u}}$ are chosen so that $F_1^{\mathrm{s,u}}(t_0,t_0) = 0$ and $\tilde{C}_0^{\mathrm{s}}$ is chosen to satisfy (5.10) so that $G_1^{\mathrm{s}}(t_0,t_0) = G_1^{\mathrm{u}}(t_0,t_0)$. Note that the choice of $C_1^{\mathrm{s,u}}$ so that $F_1^{\mathrm{s,u}}(t_0, t_0) = 0$ corresponds to adding multiples of the homogeneous solution, $C_1^{\mathrm{s,u}}\,\mathrm{d}\boldsymbol{q}_0/\mathrm{d}t$, to $\boldsymbol{q}_1^{\mathrm{s,u}}$. This is also equivalent to choosing particular values for $A^{\mathrm{s,u}}$ in the linear regime solutions in (5.1) and (5.3). Likewise, the choice of $\tilde{C}_0^{\mathrm{s}}$ so that $G_1^{\mathrm{s}}(t_0,t_0) = G_1^{\mathrm{u}}(t_0,t_0)$ corresponds to a particular choice of B in (5.1). It follows then from (A 9a) and (A 13a), after considerable manipulation, that

$$V_1^{\mathrm{u}}(t_0,t_0) - V_1^{\mathrm{s}}(t_0,t_0) = \left[\frac{\partial H}{\partial U}(\boldsymbol{q}_0(0))\right]^{-1}\int_{-\infty}^\infty \nabla H(\boldsymbol{q}_0)\cdot\boldsymbol{g}(\boldsymbol{q}_0,t)\,\mathrm{d}t, \qquad \text{(A 14)}$$

with $O(\epsilon)$ error. This agrees with (4.21) and implies (4.22) when $V_1^{\mathrm{u}}(t_0,t_0) = V_1^{\mathrm{s}}(t_0,t_0)$ so that (4.10) is satisfied.

Substitution of the resulting solutions $\boldsymbol{q}_0 + \epsilon\boldsymbol{q}_1^{\mathrm{s,u}}$ in the terms neglected in deriving (3.7), (5.4a, b) and (5.8) from (2.9) indicates that additional corrections for $\boldsymbol{q}_\epsilon^{\mathrm{s,u}}$ are $O(\epsilon^2)$ for $t\in(-\infty,t_0]$ in W_ϵ^{u} and for $t\in[t_0,\infty)$ in W_ϵ^{s}, consistent with the assumptions regarding (5.9a, b) and with the error estimates in Appendix B. This result may be shown for $U_\epsilon^{\mathrm{s,u}}$ and $F_\epsilon^{\mathrm{s,u}}$ by allowing g_1' and $g_2^{\mathrm{s,u}}$ in (A 2) and (A 11) to contain $O(\epsilon)$ error terms. It follows from (A 9) and (A 13) that the corrections to $V_1^{\mathrm{s,u}}$ and $F_1^{\mathrm{s,u}}$ are $O(\epsilon)$ and thus $O(\epsilon^2)$ to $\boldsymbol{q}_0$. For $G_\epsilon^{\mathrm{s,u}}$, we let

$$G_\epsilon^{\mathrm{s,u}} = G_{\mathrm{s}} + \epsilon G_1^{\mathrm{s,u}} + \epsilon^2 G_2^{\mathrm{s,u}}, \qquad \text{(A 15)}$$

and find

$$\frac{\mathrm{d}G_2^{\mathrm{s,u}}}{\mathrm{d}t} = -\epsilon r G_2^{\mathrm{s,u}} - (rU_{\mathrm{s}} - \tau_0)(\hat{V}_1^{\mathrm{s,u}} + U_p) - rV_0\,V_1^{\mathrm{s,u}} + V_1^{\mathrm{s,u}}\tau_1\cos\omega t + O(\epsilon). \quad \text{(A 16)}$$

Since the $O(1)$ terms on the right-hand side of (A 16) either approach zero exponentially as $t\to\infty$ in $W_\epsilon^{\mathrm{s}}(p)$ or as $t\to-\infty$ in $W_\epsilon^{\mathrm{u}}(p)$ or are multiplied by $\sin\omega t$, $\cos\omega t$, or $\sin 2\omega t$, we conclude that the particular solution of (A 16) satisfies $G_2^{\mathrm{s,u}} = O(1)$. Thus, the corrections are $O(\epsilon^2)$.

Finally, we record below L_0 derived from (A 8). From (3.7a) and (3.9a) we have

$$F_0(t-t_0) = \frac{-\alpha\gamma k \sinh k(t-t_0)}{[\beta+\gamma\cosh k(t-t_0)]^2}, \tag{A 17a}$$

where

$$\alpha = 8k^2 V_{m\pm}, \quad \beta = bV_{m\pm}, \quad \gamma = 8k^2 - bV_{m\pm}. \tag{A 17b, c, d}$$

It follows from (A 8) that

$$\begin{aligned} L_0(t-t_0) = [(\alpha\gamma k)^2 k \sinh k(t-t_0)]^{-1} [&-4\beta^3\gamma - 4\beta\gamma^3 - (\beta^4 + 6\beta^2\gamma^2 + \gamma^4)\cosh k(t-t_0) \\ &+ (6\beta^2\gamma^2 + \tfrac{3}{2}\gamma^4) k(t-t_0)\sinh k(t-t_0) + 4\beta\gamma^3 \sinh^2 k(t-t_0) \\ &+ \tfrac{1}{2}\gamma^4 \sinh^2 k(t-t_0)\cosh k(t-t_0)], \end{aligned} \tag{A 18}$$

where the constant of integration in (A 18) has been set equal to zero, since that constant simply leads to a change in $C_1^{s,u}$. In particular, we find

$$F_0(0) L_0(0) = \left[\frac{\partial H}{\partial U}(\boldsymbol{q}_0(0))\right]^{-1}. \tag{A 19}$$

Appendix B. Linear solutions near the unstable periodic oscillation

Approximate linear solutions in $W_\epsilon^s(p)$ and $W_\epsilon^u(p)$ near the unstable periodic oscillation are obtained as follows. In (2.9), let

$$(U, F, G) = (U_s, 0, G_s) + (V, F, G'), \tag{B 1}$$

where U_s and G_s are known from (3.3) and (4.3). The resulting equations for (V, F, G') are

$$\frac{dV}{dt} = F + \epsilon(-rV - rU_s + \tau_0 + \tau_1 \cos\omega t), \tag{B 2a}$$

$$\frac{dF}{dt} = k^2 V + \tfrac{3}{2}(1-U_s)V^2 - \tfrac{1}{2}V^3 + (U_s - 1 + V)G' + \epsilon(-rF), \tag{B 2b}$$

$$\frac{dG'}{dt} = \epsilon[-rG' - (rU_s - \tau_0)V - \tfrac{1}{2}rV^2 + (U_s - 1 + V)\tau_1 \cos\omega t]. \tag{B 2c}$$

Since the particular solutions of (B 2) are $O(\epsilon)$, it is natural to expand

$$(V, F, G') = \epsilon(U_1, F_1, G_1) + \epsilon^2(U_2, F_2, G_2) + O(\epsilon^3). \tag{B 3}$$

The resulting equations for (U_1, F_1, G_1) are

$$\frac{dU_1}{dt} = F_1 - rU_s + \tau_0 + \tau_1 \cos\omega t, \quad \frac{dF_1}{dt} = k^2 U_1 + (U_s - 1)G_1, \tag{B 4a, b}$$

$$\frac{dG_1}{dt} = (U_s - 1)\tau_1 \cos\omega t + \epsilon[-rG_1 - (rU_s - \tau_0 - \tau_1 \cos\omega t)U_1], \tag{B 4c}$$

where the $O(\epsilon)$ terms are retained in (B 4c) so that all leading-order linear solutions to (B 2) will be obtained. Equations (B 4) may be simplified further by substituting

$$U_1 = U_1' - \frac{(U_s - 1)}{k^2} G_1' + U_p, \tag{B 5a}$$

$$F_1 = F_1' + F_p, \quad G_1 = G_1' + G_p, \tag{B 5b, c}$$

where U_p, F_p and G_p are defined in (5.2). This gives

$$\frac{\mathrm{d}U_1'}{\mathrm{d}t} = F_1', \quad \frac{\mathrm{d}F_1'}{\mathrm{d}t} = k^2 U_1', \tag{B 6a, b}$$

$$\frac{\mathrm{d}G_1'}{\mathrm{d}t} = \epsilon\left[-rG_1' - (rU_\mathrm{s} - \tau_0 - \tau_1\cos\omega t)\left(-\frac{(U_\mathrm{s}-1)}{k^2}G_1' + U_1'\right) + a\sin\omega t + b\sin 2\omega t\right], \tag{B 6c}$$

where

$$a = \left[(rU_\mathrm{s} - \tau_0)\frac{(U_\mathrm{s}-1)^2 - \omega^2}{\omega^2 + k^2} - r(U_\mathrm{s}-1)\right]\frac{\tau_1}{\omega}, \quad b = -\frac{(U_\mathrm{s}-1)^2 - \omega^2}{2\omega(\omega^2+k^2)}\tau_1^2, \tag{B 7a, b}$$

and where the $O(\epsilon)$ term involving $\mathrm{d}G_1'/\mathrm{d}t$ has been consistently dropped in (B 6a). The first two of these, (B 6a, b), may be written in matrix form:

$$\frac{\mathrm{d}}{\mathrm{d}t}\begin{pmatrix} U_1' \\ F_1' \end{pmatrix} = \begin{pmatrix} 0 & 1 \\ k^2 & 0 \end{pmatrix}\begin{pmatrix} U_1' \\ F_1' \end{pmatrix}, \tag{B 8}$$

and solved independently of the third, (B 6c). The eigenvalues of the matrix are $\pm k$ and the corresponding eigenvectors are $(1, \pm k)$. It follows that for the eigenvalue $+k$,

$$(U_1', F_1') = (U_1'^{\mathrm{u}}, F_1'^{\mathrm{u}}) = (1, k)A^{\mathrm{u}}\exp[k(t-t_2)], \tag{B 9}$$

and for the eigenvalue $-k$,

$$(U_1', F_1') = (U_1'^{\mathrm{s}}, F_1'^{\mathrm{s}}) = (1, -k)A^{\mathrm{s}}\exp[-k(t-t_1)]. \tag{B 10}$$

G_1' is yet undetermined but enters into the solution for U_1 by (B 5a). The linear approximation (B 9) and (B 10), with (B 1), (B 3), and (B 5), to the unstable and stable manifolds W_ϵ^{u} and W_ϵ^{s} may be compared with the linear approximations (3.11a, b) to W_0^{u} and W_0^{s}.

To determine G_1' for solutions in $W_\epsilon^{\mathrm{u}}(p)$, $U_1'^{\mathrm{u}}$ from (B 9) may be substituted in (B 6c), while for solutions in $W_\epsilon^{\mathrm{s}}(p)$, $U_1'^{\mathrm{s}}$ from (B 10) is used. The result is

$$\frac{\mathrm{d}G_1'}{\mathrm{d}t} = \epsilon\left[-(r+\alpha)G_1' - \frac{(U_\mathrm{s}-1)}{k^2}\tau_1\cos\omega t\, G_1' - (rU_\mathrm{s} - \tau_0 - \tau_1\cos\omega t)A^{\mathrm{s,u}}\exp[\pm k(t-t_{1,2})] + a\sin\omega t + b\sin 2\omega t\right]. \tag{B 11}$$

It is convenient to make the substitution

$$G_1' = G_{1h} + G_{1p}, \tag{B 12}$$

where

$$G_{1p} = G_{1p}^{\mathrm{s,u}} = \epsilon\left\{\left[-\frac{(rU_\mathrm{s} - \tau_0)}{\pm k} + \frac{\tau_1}{\omega^2+k^2}(\pm k\cos\omega t + \omega\sin\omega t)\right]A^{\mathrm{s,u}}\exp[\pm k(t-t_{1,2})] - \frac{a}{\omega}\cos\omega t - \frac{b}{2\omega}\cos 2\omega t\right\}, \tag{B 13}$$

and G_{1h} satisfies

$$\frac{\mathrm{d}G_{1h}}{\mathrm{d}t} = \epsilon\left[-(r+\alpha)G_{1h} - \frac{(U_\mathrm{s}-1)}{k^2}\tau_1\cos\omega t\, G_{1h}\right]. \tag{B 14}$$

The particular solutions $G_{1p}^{\mathrm{s,u}}$ are $O(\epsilon)$, while the solution of (B 14) is

$$G_{1h} = B\exp[-\epsilon(r+\alpha)(t-t_1) - \epsilon\frac{(U_\mathrm{s}-1)}{\omega k^2}\tau_1\sin\omega t], \tag{B 15}$$

which implies $$G^{s}_{1h} = B\exp[-\epsilon(r+\alpha)(t-t_1)][1+O(\epsilon)], \tag{B 16}$$

and $$G^{u}_{1h} = 0. \tag{B 17}$$

With the substitution,

$$U_2 = U'_2 - \frac{(U_s-1)}{k^2}G_2, \tag{B 18}$$

the equations for (U'_2, F_2, G_2) are

$$\frac{dU'_2}{dt} = F_2 + R_1, \tag{B 19a}$$

$$\frac{dF_2}{dt} = k^2 U'_2 + R_2, \tag{B 19b}$$

$$\frac{dG_2}{dt} = \epsilon[-(r+\alpha)G_2 - \frac{(U_s-1)}{k^2}\tau_1\cos\omega t G_2] + \epsilon R_3, \tag{B 19c}$$

where $$R_1 = -rU_1 - \frac{(U_s-1)}{\epsilon k^2}\frac{dG'_1}{dt}, \quad R_2 = -rF_1 + \tfrac{3}{2}(1-U_s)U_1^2 + G_1 U_1, \tag{B 20a, b}$$

$$R_3 = -(rU_s - \tau_0 - \tau_1\cos\omega t)U'_2 - \tfrac{1}{2}rU_1^2. \tag{B 20c}$$

Solutions for $U_2^{s,u}, F_2^{s,u}, G_2^{s,u}$ may be readily obtained from (B 19) after substituting $(U_1^{s,u}, F_1^{s,u}, G_1'^{s,u})$ in (R_1, R_2, R_3), but these solutions are not written out here. It is clear from the form of (B 19) and of (R_1, R_2, R_3) in (B 20) that $(U_2^{s,u}, F_2^{s,u}, G_2^{s,u})$ will be well behaved and $O(1)$ in $W^s_\epsilon(p)$ for $t\in[t_1,\infty)$ and in $W^u_\epsilon(p)$ for $t\in(-\infty, t_2]$. Secular terms may be removed in the usual manner (e.g. Kevorkian & Cole 1981) by allowing $A^{s,u}$ in $(U_1'^{s,u}, F_1'^{s,u})$ to depend on ϵt, which gives

$$A^{s,u} = A_0^{s,u}\exp[-\epsilon(r+\tfrac{1}{2}\alpha)t]. \tag{B 21}$$

As a result, the leading-order approximations for solutions in $W^{s,u}_\epsilon(p)$ near the unstable periodic oscillation, as defined in (B 1), (B 3) and (B 5), are given for $W^s_\epsilon(p)$ by (B 10), (B 12) and (B 16) and for $W^u_\epsilon(p)$ by (B 8), (B 12) and (B 17) and are written out in (5.1) and (5.3).

Appendix C. Numerical solutions in $W^s_\epsilon(p)$ and $W^u_\epsilon(p)$

To calculate numerical solutions in the stable manifold $W^s_\epsilon(p)$ we utilize the variables $(V, F, G') = (U-U_s, F, G-G_s)$ and integrate (2.9) backwards in time starting at $t = t_1$, with initial conditions from (5.1):

$$V(t_1) = \epsilon\left[A^s - \frac{(U_s-1)}{k^2}B + U_p(t_1)\right], \tag{C 1a}$$

$$F(t_1) = \epsilon[-kA^s + F_p(t_1)], \tag{C 1b}$$

$$G'(t_1) = \epsilon[B + G_p(t_1)]. \tag{C 1c}$$

As a result of (5.9*a*) and (5.13) we can choose the ratio A^s/B such that in a Poincaré section we integrate approximately along that particular direction in the two-dimensional manifold $W^s_\epsilon(p)$ for which, if (4.24) is satisfied, the solutions will intersect the one-dimensional manifold $W^u_\epsilon(p)$ (figures 7, 8, and 9). From (5.1) and (5.9*a*), we obtain

$$B = \tilde{C}_0^s\exp[\epsilon(r+\alpha)(t_0-t_1)], \tag{C 2}$$

while from (3.11), with $\hat{A}^{\mathrm{s}} = \epsilon A^{\mathrm{s}}$, we find

$$k(t_0 - t_1) = \ln(\epsilon A^{\mathrm{s}}/V_{\mathrm{L}\pm}). \tag{C 3}$$

The elimination of $(t_0 - t_1)$ from (C 2) and (C 3) gives

$$B = \tilde{C}_0^{\mathrm{s}} \left(\frac{\epsilon A^{\mathrm{s}}}{V_{\mathrm{L}\pm}}\right)^{\epsilon(r+\alpha)/k}. \tag{C 4}$$

Thus, with (5.13) and (3.11 *e*), B is known in terms of ϵA^{s}. Note that for $\epsilon \to 0, B \sim \tilde{C}_0^{\mathrm{s}}$. Since for our calculation $\epsilon \ll 1$, we find typically that, even for $\epsilon A^{\mathrm{s}} \ll 1, B \approx \tilde{C}_0^{\mathrm{s}}$.

To calculate the Poincaré section for this particular set of solutions in $W_\epsilon^{\mathrm{s}}(p)$ with (C 4), we proceed as follows. We choose initially a small value of ϵA^{s} (e.g. $\epsilon A^{\mathrm{s}} = 2 \times 10^{-6}$), use (C 4) for B, assume t_1 is such that $\sin \omega t_1 = 0$, start with (C 1), and calculate the solution to a time that is one period of the forcing later, i.e. to $t_1' = t_1 + (2\pi/\omega)$, with ϵA^{s} initially chosen small enough that the solution at t_1' is still effectively in the linear regime. We then choose a large number (e.g. 2500) of initial conditions uniformly spaced in (U, F, G') between the initial values and the t_1' values and calculate numerical solutions starting these also at $t = t_1$, so that $\sin \omega t_1 = 0$. Each solution is sampled at time intervals of $(2\pi/\omega)$ to provide a point in the Poincaré section of $W_\epsilon^{\mathrm{s}}(p)$. These points are plotted in figures 11 and 12 as projections on the (V, F)-, (V, G)-, or (G', F)-planes where the individual points are connected to form continuous lines.

To calculate numerical solutions in the unstable manifold W_ϵ^{u} we integrate (2.9) forward in time starting at $t = t_2$ with initial conditions from (5.3):

$$V(t_2) = \epsilon[A^{\mathrm{u}} + U_p(t_2)], \quad F(t_2) = \epsilon[kA^{\mathrm{u}} + F_p(t_2)], \quad G'(t_2) = \epsilon G_p(t_2), \quad (C\,5a, b, c)$$

where again ϵA^{u} is small and we assume t_2 is such that $\sin \omega t_2 = 0$. The Poincaré section for $W_\epsilon^{\mathrm{u}}(p)$ is then found by plotting a large number of different solutions at time intervals of $(2\pi/\omega)$ in a manner similar to that explained above in connection with $W_\epsilon^{\mathrm{s}}(p)$.

REFERENCES

Abarbanel, H. 1983 Universality and strange attractors in internal-wave dynamics. *J. Fluid Mech.* **135**, 407–434.

Allen, J. S. 1980 Models of wind-driven currents on the continental shelf. *Ann. Rev. Fluid Mech.* **12**, 389–433.

Arnol'd, V. I. 1964 Instability of dynamical systems with many degrees of freedom. *Sov. Math. Dokl.* **5**, 581–585.

Charney, J. & DeVore, J. 1979 Multiple flow equilibria in the atmosphere and blocking. *J. Atmos. Sci.* **36**, 1205–1216.

Chow, S. N., Hale, J. K. & Mallet-Paret, J. 1980 An example of bifurcation to homoclinic orbits. *J. Diffl Equat.* **37**, 112–159.

Guckenheimer, J. & Holmes, P. 1983 *Nonlinear Oscillations, Dynamical Systems, and Bifurcations of Vector Fields.* Springer.

Hale, J. J. 1969 *Ordinary Differential Equations.* Wiley.

Hart, J. 1979 Barotropic quasi-geostrophic flow over anisotropic mountains. *J. Atmos. Sci.* **36**, 1739–1746.

Hart, J. 1985 A laboratory study of baroclinic chaos on the *f*-plane. *Tellus* **37A**, 286–296.

Hart, J. 1986 A model for the transition to baroclinic chaos. *Physica* **20D**, 350–362.

Hirsch, M. W., Pugh, C. C. & Shub, M. 1977 Invariant manifolds. Springer Lecture Notes in Mathematics, vol. 583. Springer.

Kevorkian, J. & Cole, J. D. 1981 *Perturbation Methods in Applied Mathematics.* Springer.

KLEIN, P. & PEDLOSKY, J. 1986 A numerical study of baroclinic instability at large supercriticality. *J. Atmos Sci.* **43**, 1243–1262.

LORENZ, E. N. 1963 Deterministic nonperiodic flow. *J. Atmos. Sci.* **20**, 130–141.

LORENZ, E. N. 1984 Irregularity: a fundamental property of the atmosphere. *Tellus* **36A**, 98–110.

MELNIKOV, V. K. 1963 On the stability of the center for time-periodic perturbations. *Trans. Moscow Math. Soc.* **12**, 1–57.

OHLSEN, D. R. & HART, J. E. 1989 The transition to baroclinic chaos on the β-plane. *J. Fluid Mech.* **203**, 23–50.

PEDLOSKY, J. 1981*a* The nonlinear dynamics of baroclinic wave ensembles. *J. Fluid Mech.* **102**, 169–209.

PEDLOSKY, J. 1981*b* The effect of β on the chaotic behavior of unstable baroclinic waves. *J. Atmos. Sci.* **38**, 717–731.

PEDLOSKY, J. 1987 *Geophysical Fluid Dynamics.* Springer.

PEDLOSKY, J. & FRENZEN, C. 1980 Chaotic and periodic behavior of finite amplitude baroclinic waves. *J. Atmos. Sci.* **37**, 1177–1196.

SAMELSON, R. M. & ALLEN, J. S. 1987 Quasi-geostrophic topographically generated mean flow over the continental margin. *J. Phys. Oceanogr.* **17**, 2043–2064.

ŠILNIKOV, L. P. 1965 A case of the existence of a denumerable set of periodic motions. *Sov. Math. Dokl.* **6**, 163–166.

SMALE, S. 1963 Diffeomorphisms with many periodic points. In *Differential and Combinatorial Topology* (ed. S. S. Cairns), pp. 63–80. Princeton University Press.

SMALE, S. 1967 Differentiable dynamical systems. *Bull. Am. Math. Soc.* **73**, 747–817.

SPARROW, C. 1982 *The Lorenz Equations.* Springer.

WIGGINS, S. 1988 *Global Bifurcations and Chaos: Analytical Methods.* Springer.

WIGGINS, S. & HOLMES, P. 1987 Homoclinic orbits in slowly varying oscillators. *SIAM J. Math. Anal.* **18**, 612–629 and Errata, **19**, 1988, 1254–1255.

WIGGINS, S. & SHAW, S. W. 1988 Chaos and three-dimensional horseshoes in slowly varying oscillators. *Trans. ASME* C: *J. Appl. Mech.* **55**, 959–968.

WOLF, A., SWIFT, J. B., SWINNEY, H. L. & VASTANO, J. A. 1985 Determining Lyapunov exponents from a time series. *Physica* **16D**, 285–317.